

UCSF

UC San Francisco Previously Published Works

Title

Deciphering distinct genetic risk factors for FTLD-TDP pathological subtypes via whole-genome sequencing.

Permalink

<https://escholarship.org/uc/item/4w88x0kn>

Journal

Nature Communications, 16(1)

ISSN

2041-1723

Authors

Pottier, Cyril

Küçükali, Fahri

Baker, Matt

et al.

Publication Date

2025-04-01

DOI

10.1038/s41467-025-59216-0

Copyright Information

This work is made available under the terms of a Creative Commons Attribution-NonCommercial-NoDerivatives License, available at

<https://creativecommons.org/licenses/by-nc-nd/4.0/>

Peer reviewed

Deciphering distinct genetic risk factors for FTLD-TDP pathological subtypes via whole-genome sequencing

Received: 5 June 2024

Accepted: 15 April 2025

Published online: 25 April 2025

 Check for updates

A list of authors and their affiliations appears at the end of the paper

Frontotemporal lobar degeneration with neuronal inclusions of the TAR DNA-binding protein 43 (FTLD-TDP) is a fatal neurodegenerative disorder with only a limited number of risk loci identified. We report our comprehensive genome-wide association study as part of the International FTLD-TDP Whole-Genome Sequencing Consortium, including 985 patients and 3,153 controls compiled from 26 institutions/brain banks in North America, Europe and Australia, and meta-analysis with the Dementia-seq cohort. We confirm *UNC13A* as the strongest overall FTLD-TDP risk factor and identify *TNIP1* as a novel FTLD-TDP risk factor. In subgroup analyzes, we further identify genome-wide significant loci specific to each of the three main FTLD-TDP pathological subtypes (A, B and C), as well as enrichment of risk loci in distinct tissues, brain regions, and neuronal subtypes, suggesting distinct disease aetiologies in each of the subtypes. Rare variant analysis confirmed *TBK1* and identified *C3AR1*, *SMG8*, *VIPR1*, *RBPJL*, *L3MBTL1* and *ANO9*, as novel subtype-specific FTLD-TDP risk genes, further highlighting the role of innate and adaptive immunity and notch signaling pathway in FTLD-TDP, with potential diagnostic and novel therapeutic implications.

Frontotemporal lobar degeneration (FTLD) is one of the leading causes of dementia in individuals younger than 65 years, but can also affect individuals later in life. The predominant clinical presentations of FTLD are behavioral and language dysfunction resulting in behavioral variant frontotemporal dementia (bvFTD)¹, semantic variant primary progressive aphasia (svPPA), or nonfluent variant primary progressive aphasia (nfvPPA)². The diagnosis of FTLD can be established with certainty only with neuropathologic postmortem examination and is characterized neuropathologically by significant atrophy of the frontal and temporal lobes and accumulation of abnormal neuronal and/or glial inclusions upon immunohistochemical analysis. FTLD-TDP, characterized by neuronal and cytoplasmic aggregates of the DNA and RNA-binding protein TDP-43, is one of the two main pathological subtypes (the other being FTLD-Tau) and can be further classified into five FTLD-TDP subtypes (FTLD-TDP A-E) based on the distribution of the neuronal cytoplasmic TDP-43-positive inclusions and dystrophic neurites in the cortical layers^{3,4}.

The main subtypes are types A, B, and C. Type A includes patients with moderate to numerous TDP-43-immunoreactive neuronal cytoplasmic inclusions (NCIs) and short dystrophic neurites (DNs) concentrated mainly in the upper cortical layers II/III. Type B encompasses patients with moderate to numerous TDP-43-immunoreactive NCIs and sparse DN distributed across all cortical layers. Type C is designated for patients where long dystrophic neurites are prevalent primarily in the upper cortices, and NCIs are infrequent. Extensive research is focused on the accurate prediction of the underlying FTLD neuropathology in clinical FTLD patients; however, despite some recent reports on the possible use of Tau and TDP43 levels in plasma extracellular vesicles, this remains a major diagnostic challenge⁵. Importantly, among FTLD-TDP patients, a few clinicopathological correlations exist. Specifically, FTLD-TDP C pathology is strongly overrepresented in svPPA patients⁶, whereas patients with bvFTD with concomitant amyotrophic lateral sclerosis (ALS) almost invariably present as FTLD-TDP B at autopsy^{2,4,7}.

✉ e-mail: cpottier@wustl.edu; rosa.rademakers@uantwerpen.vib.be

A small number of autosomal dominant genes and risk factors associated with FTLT-DTP have been reported^{8–14}. A quarter of FTLT-DTP patients are associated with repeat expansions in *C9orf72*, which are mainly enriched in patients with FTLT-DTP B, while autosomal dominant loss-of-function (LOF) mutations in *GRN* explain 10–15% of familial patients and invariably lead to FTLT-DTP A^{15,16}. The first FTLT-DTP genome-wide association study (GWAS) identified the *TMEM106B* locus (rs1990622); however, this signal was strongly driven by the FTLT-DTP A patients with *GRN* mutations included in that study¹⁷. Three additional FTLT-DTP loci, *UNC13A*, *DPP6*, and *HLA-DQA2*, were identified in phase I of the International FTLT-DTP whole-genome sequencing (WGS) consortium and require replication in larger datasets¹². Importantly, most FTLT-DTP patients are not yet genetically explained, and the relatively small sample size precluded rare variant analyses in phase I.

To validate and identify new genetic risk factors, we doubled the original sample size of the FTLT-DTP WGS consortium by not only sequencing more pathologically confirmed FTLT-DTP patients but also including clinically defined FTLT subtypes enriched for specific FTLT-DTP pathological subtypes at autopsy. In this work, we performed association study analyzes of both common (minor allele frequency, MAF, >1%) and rare (MAF <1%) variants, followed by comprehensive gene-prioritization, enrichment analyzes, and colocalization studies. We identify novel FTLT-DTP risk loci, including novel risk genes and loci specific to FTLT-DTP pathological subtypes. Our study highlights similarities and differences between FTLT-DTP and other neurodegenerative diseases, while unique biological processes in specific tissues, brain regions, and cell types were found to characterize individual FTLT-DTP pathological subtypes.

Results

Common variant genome-wide association analysis (GWAS)

To identify novel common FTLT-DTP genetic risk factors, we performed single variant GWAS using an additive disease risk model for 6,568,099 common variants in 985 patients and 3153 controls free of neurodegenerative disorder that passed quality control (QC). Variants

with MAF >1% in patients or controls were considered. Combining all patients (FTLT-DTP All), we identified one genome-wide significant signal at the *UNC13A* locus (rs8111424, OR = 1.37, $P = 1.17 \times 10^{-8}$). We also performed separate GWAS within the FTLT-DTP A, FTLT-DTP B, and FTLT-DTP C subtypes (Fig. 1, Tables 1–2, Supplementary Data 1, Supplementary Fig. 1). The most significant locus identified in FTLT-DTP A was *GRN* (rs5848; OR = 1.89, $P = 5.57 \times 10^{-9}$). In phase I, this locus only reached genome-wide significance under an exploratory recessive model¹², and also now, the recessive model provided an even stronger association (OR = 4.12, $P = 8.28 \times 10^{-15}$). We further detected 3 additional new genome-wide significant loci in FTLT-DTP A: *TINAG* (rs138698596), *MZT1* (rs138959102), and *FARP2* (rs886815). In FTLT-DTP B, we detected a genome-wide significant association at the *UNC13A* locus (rs12973192). The lead variant rs12973192 is in linkage disequilibrium (LD) with rs8111424 ($D' = 1$; $r^2 = 0.43$) identified in the FTLT-DTP All analysis. We further detected 3 new genome-wide significant risk loci in FTLT-DTP B: *TNIP1* (rs871269), *RCL1* (rs76742217), *PDS5B* (rs527749954), and one in FTLT-DTP C *C19orf52* (also known as *TIMM29*, rs576561313). Given the large number of svPPA patients included in the FTLT-DTP C group and the evolving literature on the exact clinicopathological correlation of this clinical subtype with FTLT-DTP C, we performed an additional association study including only pathologically confirmed FTLT-DTP C (referred to as FTLT-DTP C*, Supplementary Fig. 2). This analysis showed 4 genome-wide significant loci in *LRP1B* (rs35902922), *COL22A1* (rs146589681), *TMEM135* (rs117642163), and *TRPC4* (rs540663062). These loci were only nominally significant in the analysis including the svPPA patients (*LRP1B*: $P = 1.72 \times 10^{-4}$; OR = 4.66, *COL22A1*: $P = 0.03$; OR = 5.32; *TMEM135*: $P = 1.68 \times 10^{-3}$; OR = 2.19, and *TRPC4*: $P = 1.25 \times 10^{-4}$; OR = 2.91).

We also specifically assessed evidence for association at previously reported FTLT risk loci^{12,14,17,18}. Besides the *UNC13A* locus, which we previously identified in our Phase I study, none of the other reported risk loci were replicated at the genome-wide significance level (Supplementary Data 2). Notably, *TMEM106B* rs1990622 almost reached the genome-wide significance threshold in the FTLT-DTP A subgroup ($P = 2.7 \times 10^{-7}$, OR = 0.80).

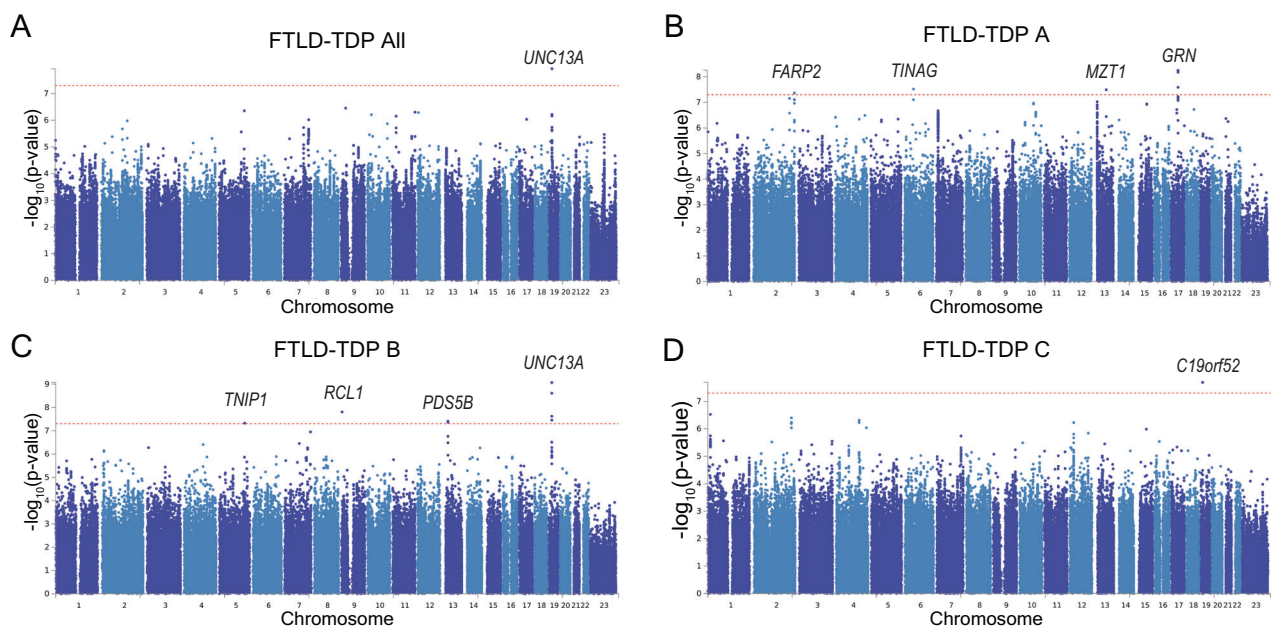


Fig. 1 | Genome-wide association study on common variants. Association studies were performed using logistic regression with allele dosage as the predictor assuming log-additive allele effects adjusted for relevant covariates. Raw two-sided P are reported as $-\log_{10}(P)$. **A** Manhattan plot of the FTLT-DTP All patients versus controls association study (inflation, $\lambda = 1.05$). **B** Manhattan plot of the FTLT-DTP A

patients versus controls association study ($\lambda = 1.07$). **C** Manhattan plot of the FTLT-DTP B patients versus controls association study ($\lambda = 1.06$). **D** Manhattan plot of the FTLT-DTP C patients versus controls association study ($\lambda = 1.05$). The red-dotted line represents the genome-wide significance level ($p = 5 \times 10^{-8}$).

Table 1 | Demographics after quality control

	FTLD-TDP A	FTLD-TDP B	FTLD-TDP C	FTLD-TDP U ^a	Control
Number (% female)	193 (42.49)	288 (38.89)	467 (48.61)	37 (40.54)	3153 (56.71)
Age at onset or age at collection (standard deviation, years)	68.00 (10.52)	62.00 (10.76)	60.50 (8.05)	60.50 (8.74)	64.08 (14.31)
Age at death (standard deviation, years)	78.00 (11.72)	67.00 (10.90)	72.00 (7.32)	67.84 (9.41)	82.00 (8.41)
Disease duration (standard deviation, years)	7.30 (4.65)	4.00 (3.61)	11.00 (7.46)	6.50 (5.20)	NA

^aFTLD-TDP U: FTLD-TDP unclassifiable.

Table 2 | Top variants associated with disease status

Group	rsid ^a	Ref/Alt	Locus name ^b	Genomic position ^c	Odds ratio (95% CI) ^d	P	MAF patients/controls	Locus name	New locus
FTLD-TDP All	rs8111424	A/G	<i>UNC13A</i>	19:17640336	1.37 (1.24–1.54)	1.17×10^{-8}	0.376/0.141	F1	
FTLD-TDP A	rs5848	C/T	<i>GRN</i>	17:44352876	1.89 (1.52–2.34)	5.57×10^{-9}	0.442/0.292	A4	New
FTLD-TDP A	rs138698596	T/A	<i>TINAG</i>	6:54591659	5.22 (2.91–9.36)	3.01×10^{-8}	0.045/0.009	A2	New
FTLD-TDP A	rs138959102	C/T	<i>MZT1</i>	13:72499532	8.41 (3.95–17.88)	3.22×10^{-8}	0.029/0.004	A3	New
FTLD-TDP A	rs886815	G/A	<i>FARP2</i>	2:241457011	9.55 (4.26–21.41)	4.26×10^{-8}	0.026/0.003	A1	New
FTLD-TDP B	rs76742217	G/A	<i>RCL1</i>	9:4821273	9.31 (4.30–20.18)	1.55×10^{-8}	0.023/0.003	B2	New
FTLD-TDP B	rs12973192	G/C	<i>UNC13A</i>	19:17642430	1.74 (1.46–2.08)	8.52×10^{-10}	0.484/0.346	B4	
FTLD-TDP B	rs527749954	C/T	<i>PDS5B</i>	13:32620689	7.66 (3.71–15.84)	3.89×10^{-8}	0.025/0.003	B3	New
FTLD-TDP B	rs871269	C/T	<i>TNIP1</i>	5:151052827	0.55 (0.44–0.68)	4.72×10^{-8}	0.206/0.322	B1	New
FTLD-TDP C	rs576561313	C/T	<i>C19orf52</i>	19:10945440	13.11 (5.33–32.23)	2.03×10^{-8}	0.014/0.001	C1	New
FTLD-TDP C*	rs540663062	A/G	<i>TRPC4</i>	13:37868802	6.35 (3.40–11.86)	6.65×10^{-9}	0.04/0.008	TC4	New
FTLD-TDP C*	rs117642163	G/T	<i>TMEM135</i>	11:87636684	5.00 (2.87–8.71)	1.37×10^{-8}	0.05/0.01	TC3	New
FTLD-TDP C*	rs35902922	T/C	<i>LRP1B</i>	2:140285968	11.86 (5.05–27.91)	1.43×10^{-8}	0.02/0.002	TC1	New
FTLD-TDP C*	rs146589681	T/A	<i>COL22A1</i>	8:139228759	10.66 (4.59–27.78)	3.80×10^{-8}	0.02/0.003	TC2	New

FTLD-TDP C*: FTLD-TDP C without svPPA.

^ars number, according to dbSNP build 153.

^bNearest protein-coding gene according to GENCODE release 33.

^cGRCh38 assembly.

^dApproximate OR calculated with respect to the alternative allele.

Gene prioritization

In order to prioritize risk genes and identify possible biological mechanisms, we applied a range of variant annotation and molecular quantitative trait loci (QTL)-GWAS integration analyzes as previously described¹⁹ on all variants (Supplementary Data 3–14). Genes included in the analyzes are listed in Supplementary Data 4. We integrated different levels of evidence using a weighting scheme and obtained a weighted sum of the hits in different subcategories for each gene. We grouped candidate risk genes in genome-wide significant loci and in subthreshold loci and prioritized them at two levels of confidence for being a likely risk gene as tier 1 (higher confidence) and tier 2 (lower confidence).

The gene prioritization analyzes nominated a total of 70 tier 1 and 286 tier 2 genes in 351 different loci for the 5 different GWAS analyzes (All, A, B, C, and C*; Fig. 2, Supplementary Data 4 and Supplementary Fig. 3–7). Our results showed that the nearest protein-coding genes were prioritized as tier 1 ($n=10$) and tier 2 ($n=3$) risk genes in the genome-wide significant loci for the distinct FTLD-TDP subtypes. Of the 10 tier 1 prioritized genes, 3 were found in common variant loci where molecular QTL-GWAS analyzes aided their prioritization (Fig. 2). First, in locus A4, *GRN* was prioritized through consistent expression QTL (eQTL) domain hits in bulk brain regions (eQTL $P_{\text{ROSMAP DLPFC}} = 6.32 \times 10^{-38}$ and $\beta_{\text{ROSMAP DLPFC}} = -0.25$, eQTL colocalization (coloc) PPH4s of 81.8%–99.7%, and fine-mapped [posterior inclusion probability being 100%] expression transcriptome-wide association study [eTWAS] associations with P from 1.74×10^{-8} to 5.15×10^{-9} and Z -scores from -5.63 to -5.84) and in oligodendrocytes (cell type specific eQTL (ct-eQTL) coloc PPH4 = 90%) where genetic downregulation of *GRN* gene expression was associated with the FTLD-TDP A risk signal

(Supplementary Data 6, 7, and 12), which was also observed in brain proteome-wide association study (PWAS) with the same effect direction for the FTLD-TDP A risk ($P_{\text{ROSMAP DLPFC}} = 3.32 \times 10^{-6}$, $Z_{\text{ROSMAP DLPFC}} = -4.65$, Supplementary Data 14). Second, in locus B1, *TNIP1* was prioritized because the minor allele was associated with decreased *TNIP1* expression ($P_{\text{ROSMAP DLPFC}} = 2.40 \times 10^{-4}$, $\beta_{\text{ROSMAP DLPFC}} = -0.10$), the GWAS signal colocalized with a microglia splicing QTL (sQTL) associated with *TNIP1* chr5:151032383-151035002 known splice junction (coloc PPH4 = 82.2%), and because the mQTL variants for cg03340667, a CpG -3.7 kb upstream of the transcription start site (TSS) of the canonical transcript of *TNIP1*, colocalized with the GWAS variants (coloc PPH4 = 70%) in dorsolateral prefrontal cortex (DLPFC) (Supplementary Data 6, 8, and 9). Third, in locus B4, *UNC13A* was prioritized through an eQTL-GWAS colocalization in temporal cortex (coloc PPH4 = 81.82%, Supplementary Data 7). Furthermore, beyond genome-wide significant loci, we identified additional candidate prioritized risk genes in subthreshold regions through molecular QTL-GWAS coloc and TWAS analyzes, one important example being *TMEM106B* as the prioritized risk gene in locus A_S14. The FTLD-TDP A GWAS signal near *TMEM106B* colocalized with eQTL variants regulating *TMEM106B* gene expression in bulk brain regions (eQTL coloc PPH4s = 81.40% in MayoRNASeq temporal cortex and 89.66% in Genotype-Tissue Expression (GTEx) brain cortex, Supplementary Data 7). We also observed a significant eTWAS association in GTEx cortex ($P = 4.13 \times 10^{-7}$, $Z = -5.06$), together with a significant PWAS hit ($P = 2.01 \times 10^{-8}$, $Z_{\text{score}} = 5.61$) (Supplementary Data 12, 13). Finally, a significant hit in splicing TWAS in cortex (sTWAS, $P = 6.66 \times 10^{-7}$, $Z = -4.97$) predicted a decreased preference for the *TMEM106B* splice junction chr7:12224385-12229679 with the increased FTLD-TDP A

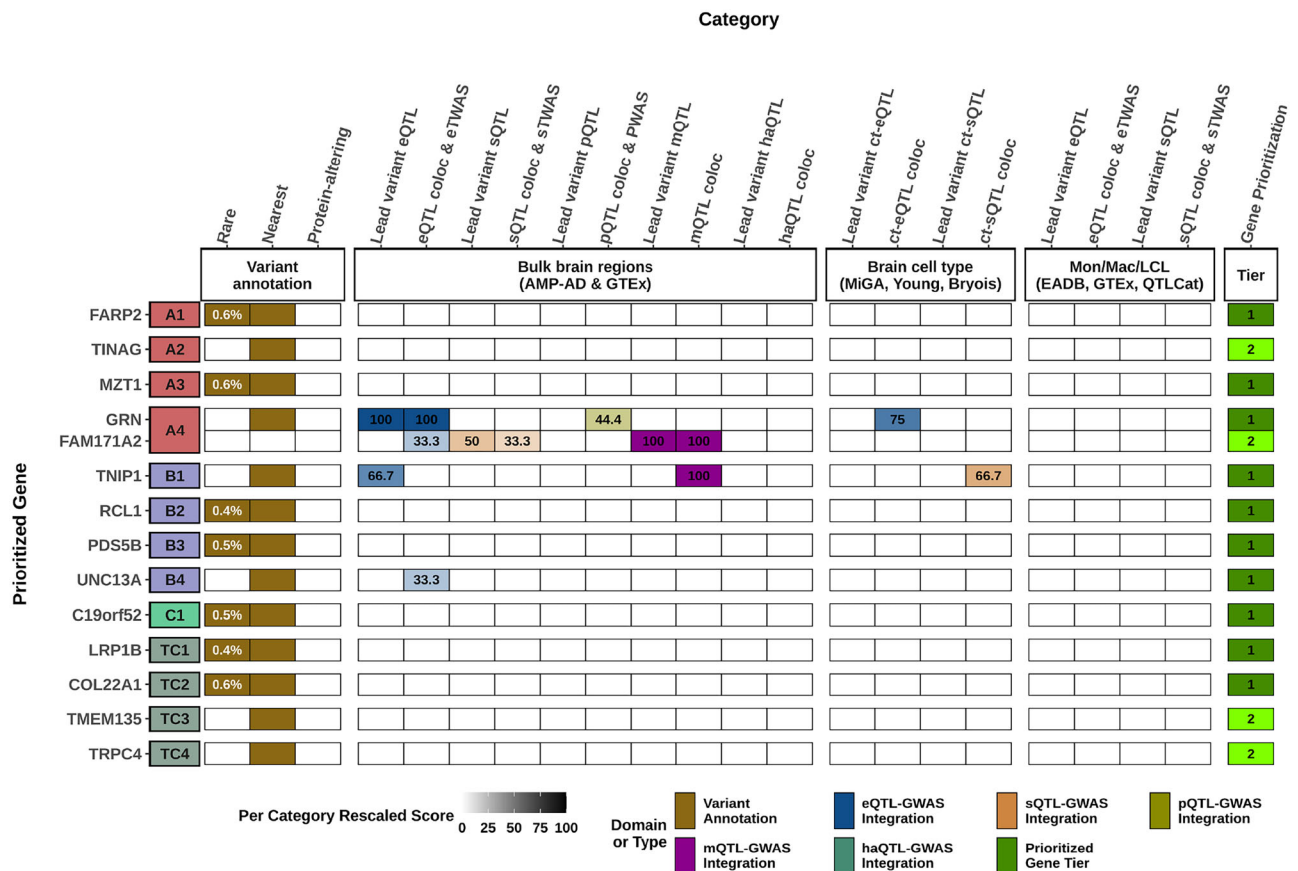


Fig. 2 | Gene prioritization results for FTLD-TDP subgroups. A visual summary of weighted evidence category scores for the prioritized genes within genome-wide significant loci in related FTLD subtype-specific GWAS summary statistics. Using the gene prioritization strategy in these selected loci, we prioritized a total of 13 genes in 12 genome-wide significant loci at two different confidence levels (10 tier 1 and 3 tier 2 prioritized genes). The leftmost squares, which are colored in red for FTLD-TDP A, in blue for FTLD-TDP B, in lighter green for FTLD-TDP C, and in darker green for FTLD-TDP C* specific analyzes, indicate the locus index numbers for the genome-wide loci. The types of evidence for each category are colored according to the six different domains to which they belonged. Weighted scores for each evidence category are rescaled to a 0–100 scale based on the maximum score a candidate gene can obtain from a category (see Supplementary Data 3). The darker

colors represent higher scores in categories, while tier 1 prioritized genes are displayed in dark green, and tier 2 prioritized genes are displayed in light green. Only tier 1 and tier 2 genes are shown for each locus, whereas all candidate genes considered and scored can be found in Supplementary Data 4. MAFs (based on gnomAD v4 non-Finnish European samples) and CADD (v1.7) PHRED scores for rare and/or protein-altering rare variants are labeled in white within the respective squares. eQTL expression QTL, sQTL splicing QTL, mQTL methylation QTL, pQTL protein-expression QTL, haQTL histone acetylation QTL, coloc colocalization, eTWS expression transcriptome-wide association study, sTWS splicing transcriptome-wide association study, PWAS proteome-wide association study, Mon Mac monocytes and macrophages, LCL lymphoblastoid cell line, QTLcat the eQTL catalog.

GWAS risk, while we also observed methylation QTL (mQTL) coloc hits for two CpGs for *TMEM106B* (-500 bp upstream cg23422036 coloc PPH4 = 94.25% and intronic cg09613507 coloc PPH4 = 94.09%) (Supplementary Data 13, 9). We summarized our gene prioritization results in Fig. 2 for the genome-wide significant loci, and full results for all performed genome-wide association studies are presented in Supplementary Data 4–14 and Supplementary Fig. 3–7.

Pathway analyzes

Next, we performed gene ontology (GO) analyzes on tier 1 prioritized genes, separately for each GWAS. The most significant term in the nominated genes in FTLD-TDP All was positive regulation of defense response to bacterium ($P = 3.98 \times 10^{-5}$). Lysosomal function appeared to be strongly affected in FTLD-TDP A with several genes such as *GRN* and *TMEM106B* (lysosomal organization GO term, $P = 4.12 \times 10^{-4}$) as well as cathepsin B (*CTSB*). We further detected enriched terms for retrograde transport in FTLD-TDP B ($P = 2.21 \times 10^{-3}$) driven by *DENND2A* and *VP53* genes, and for excitatory postsynaptic potential in FTLD-TDP C ($P = 1.48 \times 10^{-3}$) driven by *DMPK* and *P2RX5* genes (Fig. 3 and Supplementary Data 15). Note that some genes belong to multiple significant GO terms; for instance, *GRN* is present in terms associated

with FTLD-TDP A and B (Supplementary Data 15 and Supplementary Fig. 8). Finally, in the FTLD-TDP C* analysis (excluding svPPA patients), an enrichment for genes implicated in cellular homeostasis terms was observed ($p = 8.77 \times 10^{-03}$), driven by *DMPK*, *CYBA*, and *CTRC* (Supplementary Data 15 and Supplementary Fig. 2). Importantly, except for lysosomal transport, no terms overlapped between subtypes of FTLD-TDP, suggesting mostly distinct genetic etiologies in the different FTLD-TDP groups.

To further characterize genetic factors associated with FTLD-TDP, we performed gene-based analyzes on common variants with $P < 10^{-5}$ using MAGMA. Analyzes of FTLD-TDP All did not yield exome-wide significant loci; however, FTLD-TDP A showed exome-wide significant signals for the two genes located at the *GRN* locus (*FAM171A2*, *ITGA2B*) and for *TMEM106B* ($P = 4.74 \times 10^{-7}$). The *TMEM106B* signal was driven by the rs10281425 variant ($OR = 0.54$, $P = 2.12 \times 10^{-7}$). No exome-wide significant signal was detected for the other FTLD-TDP pathological subtypes (FTLD-TDP B, C, and C*).

Cell type and brain region expression pattern of GWAS hits

To find tissues and cell types for which gene expression profiles were enriched for genes within FTLD-risk loci, we combined gene-based

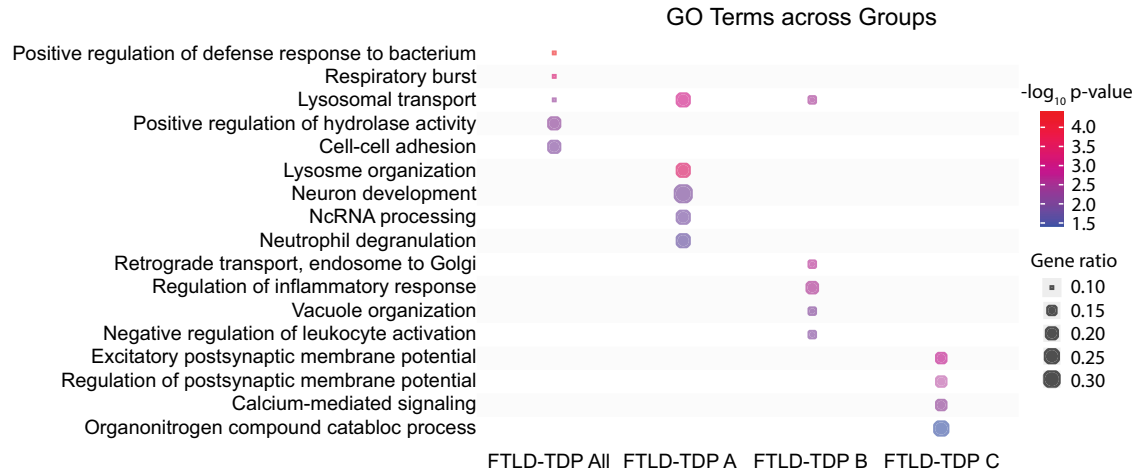


Fig. 3 | Top 5 Gene Ontology terms enriched in FTLT-DTP subgroups. Hierarchical GO analysis of biological process terms considering genes in genetic loci prioritized for FTLT-DTP All, FTLT-DTP A, FTLT-DTP B, and FTLT-DTP C. Raw two-sided *p* values are represented.

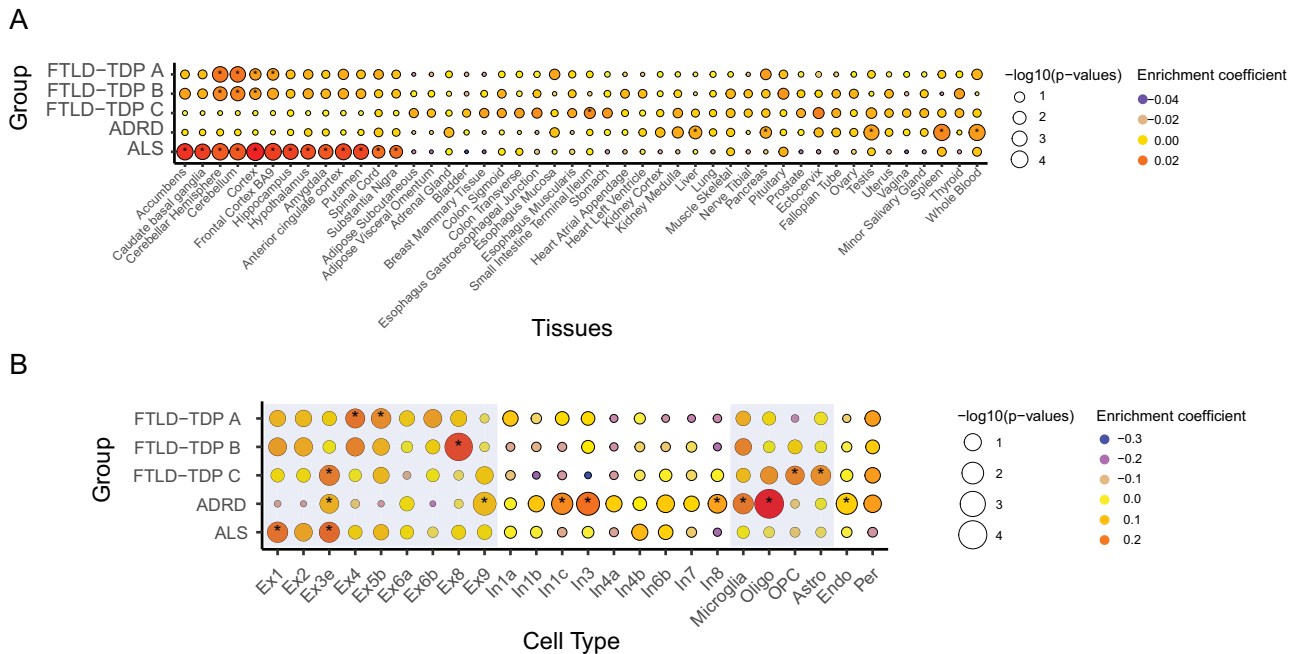


Fig. 4 | Enrichment of brain regions and cell types in FTLT subgroups. **A** Enrichment of genes in multiple tissues, including 13 brain regions, and based on GTEx data in FTLT subgroups, ADRD, and ALS. Color represents the enrichment coefficient, and size indicates two-sided $-\log_{10}$ (FDR-adjusted *P*s) of enrichment obtained by the linear regression model in the MAGMA gene property analysis. **B** Central nervous system cell type enrichment analyzes in FTLT subgroups, ADRD, and ALS. Color represents the enrichment coefficient, and size indicates two-sided

$-\log_{10}$ (FDR-adjusted *P*s) of enrichment obtained by the linear regression model in the MAGMA gene property analysis. Excitatory neurons and glial cells are highlighted in blue. Excitatory and inhibitory neurons from the PsychENCODE dataset were labeled based on their transcriptional profile from 1 to 8. Asterisks denote brain regions or cell types enriched with FDR *P* < 0.05. Cx cortex, Ex* Excitatory neuron, In* inhibitory neurons, Oligo oligodendrocytes, OPC oligodendrocyte progenitor cells, Astro astrocytes, Endo endothelial cells, Per pericytes.

association statistics calculated using MAGMA with gene expression patterns from the GTEx project in a gene set enrichment analysis. Only loci with $P < 10^{-5}$ for their respective traits were included. We observed an enrichment in genes expressed in brain tissue (cerebellum, frontal cortex, and cortex) in FTLT-DTP A and B (Fig. 4 and Supplementary Data 16). This was strikingly different from the signature observed in FTLT-DTP C, for which significant enrichment was only detected in non-central nervous system tissue, in particular small intestine terminal ileum (Fig. 4 and Supplementary Data 16). When removing svPPA patients (FTLT-DTP C* analysis), we again observed an enrichment in genes expressed in brain tissue, albeit without specificity for the frontal cortex (Supplementary Fig. 2). We also compared expression

profiles of the genes at FTLT loci with expression of genes located at associated loci in Alzheimer’s disease and related disorders (ADRD)¹⁹ and ALS GWAS²⁰ using available summary statistics and restricting our query to loci with $P < 10^{-5}$ for their respective traits. FTLT-DTP subtypes presented with a distinct genetic signature as compared to these related disorders, highlighting the importance of regional specificity in FTLT-DTP.

We subsequently queried PsychENCODE frontal-cortex single-cell RNA-seq datasets of human-derived brain samples to specify further which brain-specific enriched cell types express the genetic loci associated with FTLT-DTP risk (Fig. 4 and Supplementary Data 17). We observed a significant enrichment in genes expressed in excitatory

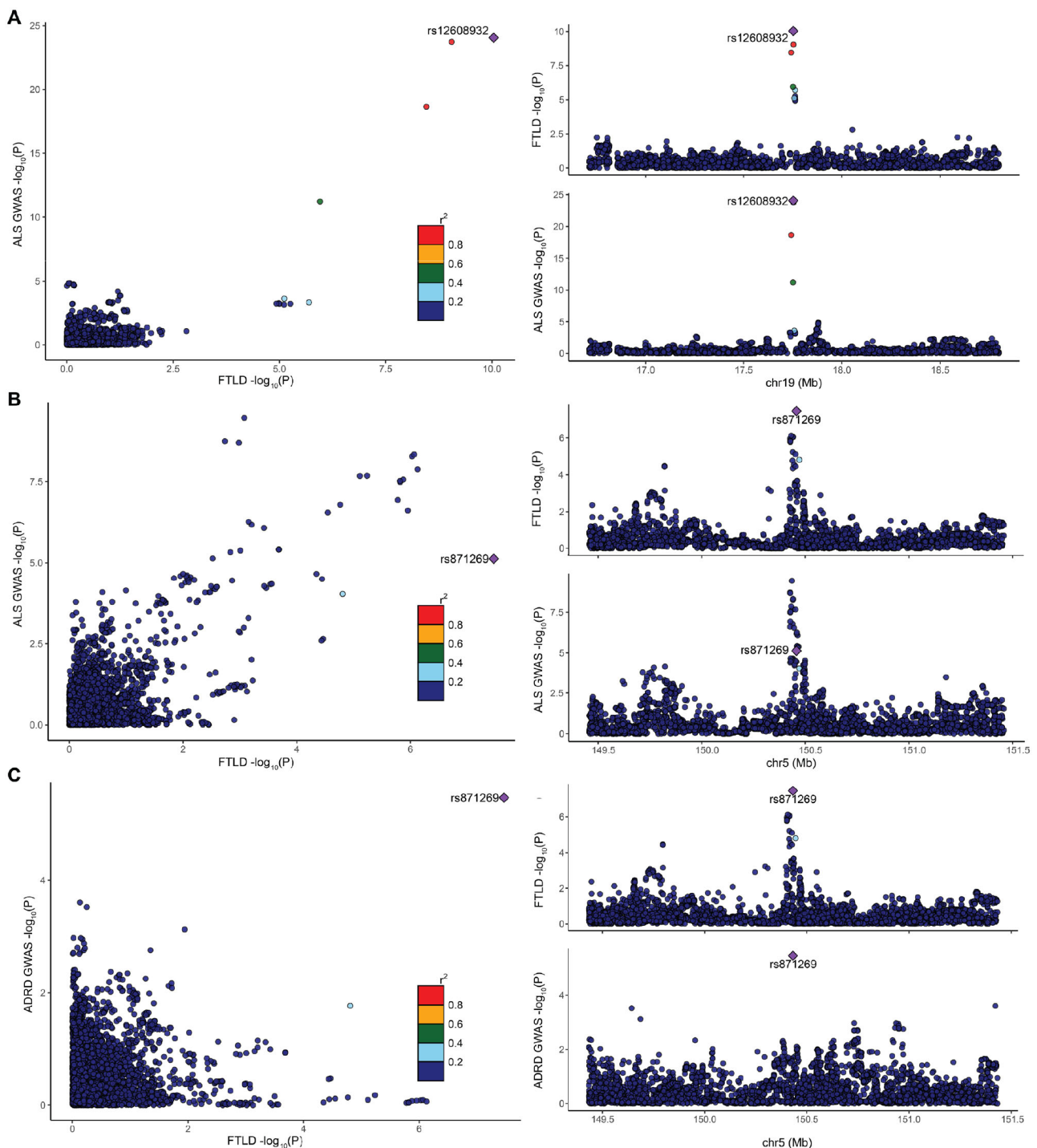


Fig. 5 | Locus zoom plots for *UNC13A* and *TNIP1* loci. **A** Genetic colocalization between the *UNC13A* locus in FTLD (meta-analysis) and ALS signal. **B** Genetic colocalization between the *TNIP1* locus in FTLD (meta-analysis) and ALS. **C** Genetic colocalization between the *TNIP1* locus in FTLD (meta-analysis) and ADRD. For

A, B, C, chromosome position is located on the x-axis, and $-\log_{10}$ transformed raw two-sided P is represented on the y-axis. Each dot represents a SNV tested in the dataset for its association with disease status. Purple diamonds are the index SNVs reported. Linkage disequilibrium with index SNV is indicated by r^2 .

neurons for FTLD-TDP A loci (Ex4 $P=3.55 \times 10^{-2}$, Ex5b $P=2.72 \times 10^{-2}$), and FTLD-TDP B loci (Ex8 $P=1.27 \times 10^{-4}$), while no other cell type reached significance. While FTLD-TDP C loci were also significantly enriched in genes expressed in excitatory neurons (Ex3e $P=2.10 \times 10^{-2}$), they were additionally enriched in genes expressed in astrocytes and oligodendrocyte progenitor cells ($P=2.53 \times 10^{-2}$, $P=4.69 \times 10^{-2}$). No significant enrichment was detected for FTLD-TDP C* (without svPPA) (Supplementary Fig. 2). Genes expressed in microglia were enriched only in ADRD gene loci ($P=1.90 \times 10^{-2}$). Overall, loci comprising genes

expressed in excitatory neurons were enriched in the three FTLD-TDP subtypes, with stronger specificity for specific neuron types in each FTLD-TDP subtype as compared to what was observed for ALS gene loci.

GWAS meta-analysis

To provide further support for the identified FTLD-TDP risk loci, we performed a meta-analysis of our FTLD-TDP cohort with the Dementia-seq study (phs001963.v1.p1), which includes 2102 clinical FTLD patients and 1748 controls. Given that this cohort lacks details on the

Table 3 | Genes harboring rare variants associated with FTLT-DTP

Group	Gene name	Number of variants	Number of patients	cMAF ^a in patients	Number of controls	cMAF ^a in controls	P
FTLD-TDP ALL	<i>TBK1</i>	9	9	4.57×10^{-3}	0	0	1.05×10^{-6}
FTLD-TDP A	<i>TBK1</i>	3	3	7.77×10^{-3}	0	0	1.27×10^{-11}
FTLD-TDP A	<i>C3AR1</i>	3	3	7.77×10^{-3}	4	6.34×10^{-4}	6.51×10^{-7}
FTLD-TDP A	<i>SMG8</i>	4	3	7.77×10^{-3}	1	1.59×10^{-4}	9.11×10^{-7}
FTLD-TDP B	<i>TBK1</i>	5	5	8.68×10^{-3}	0	0	3.17×10^{-12}
FTLD-TDP B	<i>VIPR1</i>	4	3	5.21×10^{-3}	1	1.59×10^{-4}	4.65×10^{-7}
FTLD-TDP C	<i>RBPJL</i>	6	5	5.35×10^{-3}	3	4.76×10^{-4}	6.39×10^{-7}
FTLD-TDP C	<i>L3MBTL1</i>	9	8	8.57×10^{-3}	3	4.76×10^{-4}	2.38×10^{-7}
FTLD-TDP C	<i>ANO9</i>	5	8	8.57×10^{-3}	6	9.52×10^{-4}	1.39×10^{-6}
FTLD-TDP C*	<i>ANO9</i>	4	4	1.01×10^{-2}	6	9.52×10^{-4}	1.50×10^{-6}

^acMAF cumulative minor allele frequency.

FTLD pathology underlying each patient, pathological subgroup analyzes could not be performed. Meta-analysis confirmed *UNC13A* and identified the new *TNIP1* locus as genome-wide significantly associated with FTLD ($P_{rs12973192} = 8.85 \times 10^{-10}$; $P_{rs871269} = 3.42 \times 10^{-8}$, respectively). Note that the most significant single-nucleotide variant (SNV) at the *UNC13A* locus was rs12608932 ($P = 9.13 \times 10^{-11}$), in strong LD with rs12973192 ($r^2 = 0.96$, $D' = 0.99$). Interestingly, while the *TNIP1* signal in FTLD-TDP All was not genome-wide significant, it became significant when running the meta-analysis. The change in significance likely results from the inclusion of participants with bvFTD/ALS (with likely FTLD-TDP B pathology) as part of the DementiaSeq cohort.

Overlap with other neurodegenerative diseases

Both *UNC13A* and *TNIP1* were previously associated with other neurodegenerative diseases^{19,21}. Colocalization analyzes showed that our *UNC13A* signal was shared with ALS (coloc PPH4 = 95.71%) (Fig. 5A). On the contrary, for *TNIP1*, we found strong colocalization with the ADRD association signal^{19,21} (coloc PPH4 = 99.2%) and a weaker colocalization with ALS (71.5%), which was confirmed in a sensitivity analysis (coloc PPH4 = 20.1%, for $\pi 2 = 1.00 \times 10^{-6}$), possibly reflecting multiple independent association signals in FTLD in this locus (Fig. 5B, C). Prompted by these findings, we performed global genetic correlations between FTLD-TDP (using FTLD-TDP All) and ALS and ADRD GWAS. A strong overall genetic correlation was observed between FTLD-TDP and ALS ($P = 1.88 \times 10^{-4}$, $r = 0.88$, standard error = 0.23), whereas no significant correlation was seen between FTLD-TDP and ADRD ($P = 3.1 \times 10^{-1}$, $r = 0.22$, standard error = 0.31).

Rare variant analysis

To identify genes carrying rare variants contributing to FTLD-TDP, we performed a burden test in genes with rare variants (MAF < 1% in patients or controls; Supplementary Fig. 9) likely to affect protein function. Only variants that are frameshift (insertion/deletion/block substitution), stopgain, stoploss, and splicing SNVs (jointly defined as LOF variants), and non-synonymous SNVs with a REVEL pathogenicity prediction score above 0.75²² were included. In the FTLD-TDP All cohort, no exome-wide significant gene was detected except the known *TBK1* risk gene (Table 3 and Supplementary Data 18). Even though we detected some inflation in our association tests, likely due to small cohort size, we did detect nine exome-wide significant signals within FTLD-TDP pathological subtypes (Table 3 and Supplementary Data 19–22). *TBK1* was associated with disease status in FTLD-TDP A and B ($P = 1.27 \times 10^{-11}$, inflation = 2.18; $P = 3.17 \times 10^{-12}$, inflation = 1.49, respectively, Supplementary Fig. 9). The signal was driven by 3 carriers in FTLD-TDP A patients (3/193 = 1.5%) and 5 carriers in FTLD-TDP B patients (5/288 = 1.7%) with no carriers in controls. We further identified 2 new genes in FTLD-TDP A (Supplementary Data 19) that were exome-wide significant: *C3AR1* ($P = 6.51 \times 10^{-7}$, 3/193 FTLD-TDP A and 4/

3153 controls) and *SMG8* ($P = 9.11 \times 10^{-7}$, 3/193 FTLD-TDP A and 1/3153 controls). We also detected an enrichment in rare variants in *VIPR1* in FTLD-TDP B ($P = 4.65 \times 10^{-7}$, 3/288 FTLD-TDP B and 1/3153 control; Fig. 6 and Supplementary Data 20) and 3 exome wide significant signals in FTLD-TDP C (inflation = 1.51, Supplementary Data 21 and Supplementary Fig. 9): *L3MBTL1* ($P = 2.87 \times 10^{-7}$, 8/467 FTLD-TDP C and 3/3153 controls), *RBPJL* ($P = 6.39 \times 10^{-7}$, 5/467 FTLD-TDP C and 3/3153 controls) and *ANO9* ($P = 1.39 \times 10^{-6}$, 8/467 FTLD-TDP C and 6/3153 controls). For FTLD-TDP C* (without svPPA) only *ANO9* reached exome-wide significance ($P = 1.5 \times 10^{-6}$, 4/199 FTLD-TDP C and 6/3153 controls; Supplementary Data 22). Rare variants in significantly associated genes can be found in Supplementary Data 23. Weighted gene coexpression network analysis using the ROSMAP dataset and the BrainExp database²³ revealed that *L3MBTL1* and *RBPJL* belonged to the same module (yellow, $P_{L3MBTL1} = 1.32 \times 10^{-45}$, $P_{RBPJL} = 1.00 \times 10^{-79}$; Supplementary Fig. 10) that is enriched in neuroactive ligand-receptor interaction and the cytokine-cytokine receptor interaction GO terms ($P_{FDR} = 3.7 \times 10^{-12}$, $P_{FDR} = 5.8 \times 10^{-12}$, respectively). While expression of *L3MBTL1* was throughout the central nervous system cells, *RBPJL* expression was restricted to inhibitory neurons and in particular, to Parvalbumin neurons (Supplementary Fig. 10). None of the rare variant carriers had a mutation in a known FTLD gene.

Discussion

In this work, we report 12 new genome-wide significant FTLD-TDP risk loci and 6 new genes harboring rare variants contributing to FTLD-TDP risk by performing the largest FTLD-TDP WGS study to date, including 985 patients and 3153 controls. A comprehensive analysis of our data highlights the genetic overlap between FTLD-TDP, ADRD, and ALS while also defining tissue and cell type enrichment unique to FTLD-TDP. Most importantly, we highlight distinct genetic aetiologies for each of the three main FTLD-TDP pathological subtypes (A, B, and C), suggesting that multiple distinct pathomechanisms underlie the TDP-43 dysfunction and deposition in FTLD-TDP. A graphical summary of the significant findings across FTLD-TDP subtypes can be found in Fig. 7.

We replicate in an independent cohort for the first time, our previously reported GWAS signal at the *UNC13A* locus in FTLD-TDP patients¹². This locus was also reported in a recent large GWAS focused on clinical FTLD patients and controls without reaching genome-wide significance ($P = 1.07 \times 10^{-3}$), possibly due to the heterogeneity of the underlying pathologies in this cohort, with only a subset having TDP-43 pathology¹⁸. The same *UNC13A* locus was previously linked to ALS²⁴ and is known to modify the phenotype in ALS patients by increasing the risk of frontotemporal cortical atrophy and diminished cognitive performance, which are reminiscent of an FTLD clinical presentation²⁵. From a biological perspective, the *UNC13A* risk haplotype tagged by rs12973192 and rs12608932 was previously shown to increase cryptic

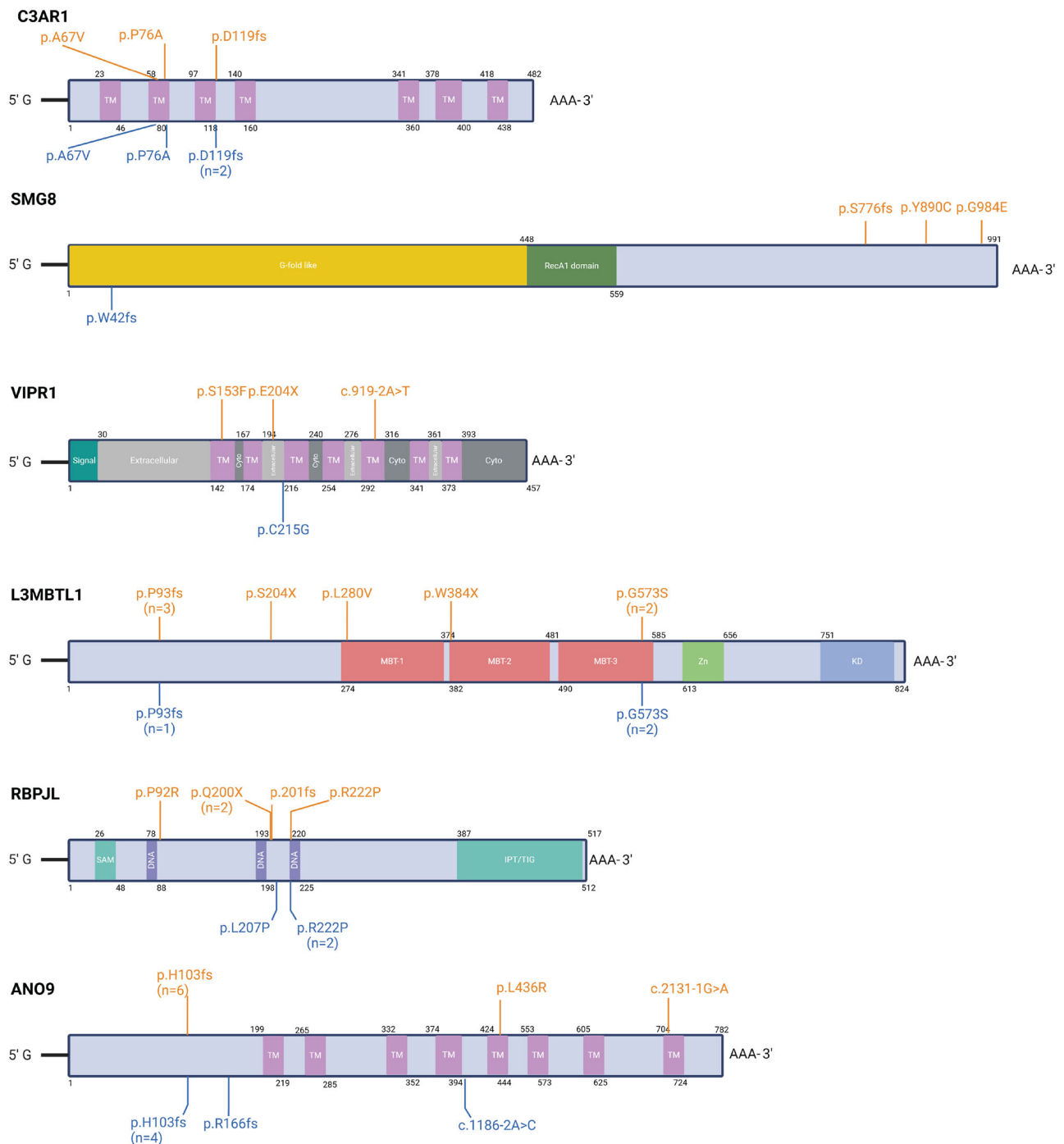


Fig. 6 | Rare loss of function and predicted pathogenic variants in proteins associated with FTLT. Schematic representation of C3AR1, SMG8, VIPR1, L3MBTL1, and RBPJL protein structure (source Uniprot) showing a map of nonsense, splicing, frameshift, and missense rare variants with a REVEL score > 0.75 in patients and controls. Variants identified in patients are colored in orange, and variants

identified in controls are colored in blue. n = number of carriers. When no number is indicated, the variant was observed in a single individual. Total number of subjects included in the analyzes was FTLT-TDP A (n = 193), FTLT-TDP B (n = 288), FTLT-TDP C (n = 467), and FTLT-TDP C* (n = 199), and controls (n = 3153).

splicing of *UNC13A* in brain tissue by modulating TDP-43 binding^{26,27}. This cryptic splicing leads to transcripts with premature stop codons and the subsequent loss of *UNC13A* protein, significantly impacting the release of vesicles in glutamatergic synapses²⁸. *UNC13A* variants thus enhance the effect of TDP-43 dysfunction, yet both ALS and FTLT-TDP are characterized by TDP-43 pathology, suggesting that additional genetic or environmental mechanisms must exist to explain the tissue specificity of the pathology and associated clinical phenotypes in individual patients.

We further establish and replicate in an independent cohort a novel genetic association between the *TNIP1* locus and FTLT-TDP. Recently, Restuadi et al. deeply characterized the *GPX3/TNIP1* locus associated with ALS and suggested that *GPX3* should be prioritized for deeper exploration into disease mechanisms related to this region²⁹. *GPX3*, encoding for glutathione peroxidase 3, is a secreted enzyme involved in the regulation of oxidative damage, and its levels were found to be reduced in ALS sera³⁰. Interestingly, however, the risk variant associated with FTLT-TDP (rs871269) is an expression

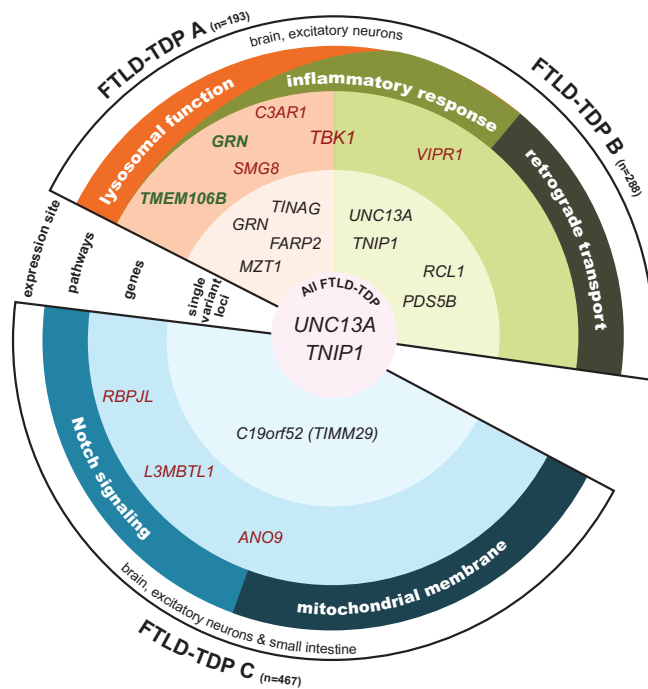


Fig. 7 | Schematic representation of findings from the International FTLD-TDP WGS phase II. Genome-wide significant single variant loci, exome-wide significant genes, enriched gene ontology pathways, and tissues- and cell-types enriched for genome-wide significant risk loci are shown for each FTLD-TDP pathological subtype in rings moving from the center (genome-wide significant single variant loci in FTLD-TDP All) to the outer rings. Orange background shades correspond to FTLD-TDP A findings, green background shades to FTLD-TDP B findings, and blue background shades to FTLD-TDP C findings. Gene names in green font were exome-wide significant using a gene-based approach with common variants, while gene names in red font were exome-wide significant using a gene-based approach with rare variants. In addition to unique associations, some overlap between FTLD-TDP A and B exists (*TBK1*, lysosomal function, and inflammatory response), whereas FTLD-TDP C showed a unique and non-overlapping genetic profile. Note that genetic associations with *LRP1B*, *COL22A1*, *TRPC4*, and *TMEM135* (identified in the FTLD-TDP C* GWAS focused solely on pathologically confirmed FTLD-TDP C patients) are not shown.

quantitative trait locus for *TNIP1* in the dorsolateral prefrontal cortex, and along with the fact that we only observed a weak colocalization signal with the ALS locus, we highlight *TNIP1*, and not *GPX3*, as the most likely gene candidate for FTLD-TDP. In fact, we observed a shared signal at this locus between our FTLD-TDP GWAS and the recent large ADRD GWAS¹⁹, whereas independent *TNIP1* association signals were reported for ALS and ADRD³¹. The genetic overlap between FTLD-TDP and AD at this locus is of interest and suggests that *TNIP1*, an important ubiquitin-binding adaptor protein regulating cell death and innate immune responses through NF- κ B activation^{32–34}, modifies a disease process shared by AD and FTLD-TDP. The idea of a continuum of neurodegenerative disorders in which common pathological mechanisms are involved is further supported by recent GWAS^{19,35}. Interestingly, *TNIP1* undergoes phosphorylation by *TBK1* and interacts with *OPTN*³⁶, two proteins associated with FTLD-TDP etiology^{13,37}. While this functional connection further supports *TNIP1* as an FTLD-TDP risk gene, more work is needed to understand the mechanisms underlying disease onset. Overall, we substantiate the genetic overlap between ALS, ADRD, and FTLD-TDP and emphasize the need for deeper exploration into pathways underlying disease-specific risk.

One of the most striking conclusions from this phase II FTLD-TDP GWAS is the distinct association signals among FTLD-TDP pathological subtypes. Even the *UNC13A* and *TNIP1* risk loci, which reach genome-

wide significance in the meta-analysis stage, show stronger association in FTLD-TDP B alone, and for the first time, genome-wide significant common risk loci are reported for each of the individual pathological FTLD-TDP subtypes.

In FTLD-TDP A, in addition to individual genome-wide significant common variants assigned to *GRN*, *TINAG*, *MZT1*, and *FARP2* risk loci, we identified exome-wide significant association with the burden of common variants in *GRN* and *TMEM106B*, in addition to multiple QTL-based analyzes prioritizing *TMEM106B* as a tier 1 risk gene, reinforcing the specific connection of these genes with FTLD-TDP A, even in patients without LOF *GRN* mutations^{12,15}. While *GRN* and *TMEM106B* are also reported as AD risk genes¹⁹, an even stronger connection exists between these genes and limbic-predominant age-related TDP-43 encephalopathy (LATE)^{38,39}, which has a more restricted neuroanatomical distribution of TDP-43 pathology as compared to FTLD-TDP but with some characteristics of FTLD-TDP A^{40,41}. The *TMEM106B* signal is primarily influenced by rs10281425, a variant located in the 3'UTR of *TMEM106B*, which tags the previously reported *TMEM106B* risk haplotype¹⁷ associated with an increase in *TMEM106B* mRNA expression¹⁷ and a higher burden of insoluble disease-associated *TMEM106B* C-terminal fragments⁴². The *GRN* association is driven by rs5848, a variant located in the 3'UTR of *GRN*, which was shown to partially reduce plasma and CSF progranulin levels, independent of the presence of *GRN* LOF mutations^{43,44}. More broadly, also including prioritized genes from the subthreshold regions, GO analysis in FTLD-TDP A revealed enrichment in genes implicated in lysosomal function driven by *GRN*, *TMEM106B*, but also *CSTB*, three genes which also had the highest individual gene scores in the prioritization analysis in FTLD-TDP A. *CSTB* encodes one of the most abundant lysosomal proteases in the brain⁴⁵, and has been reported as a progranulin protease^{46,47}. Genes involved in lysosomal dysfunction were also overrepresented in FTLD-TDP B, including *GRN* and *PPT1*. *PPT1* is a lysosomal enzyme that facilitates the degradation of fatty-acylated proteins by lysosomal hydrolases. Mutations in *PPT1* cause neuronal ceroid lipofuscinosis^{148,49}, and *Ppt1* knock-out mice displayed fewer lipid droplets (LD) than wild type, indicating impairment of lipophagy, previously associated with FTLD/ALS^{50–53}. Overall, our genetic data provide compelling evidence that lysosomal dysfunction contributes to the pathobiology of FTLD-TDP A, and, to a lesser extent, FTLD-TDP B.

For FTLD-TDP B, additionally, we identified individual genome-wide significant associations with variants in the *RCL1* and *PDS5B* loci, and we observed enrichment for GO terms related to retrograde transport resulting from the *VPS53* and *DENND2A* loci. *VPS53* is part of the Golgi-associated retrograde protein (GARP) complex^{54,55} involved in intracellular cholesterol transport by targeting NPC2 to lysosomes⁵⁶. Recently, laser capture microdissection and single-cell mass spectrometry-based proteomics in motor neurons of ALS patients revealed a strong reduction in endolysosomal trafficking complexes, such as the GARP complexes⁵⁷. Limited information about DENND2A function is currently available, but structural and functional analysis indicate it may be involved in intracellular vesicle trafficking to the lysosome and to the Golgi through its guanine nucleotide exchange factor activity and regulation of RAB family GTPases⁵⁸. However, retrograde transport has been previously implicated in ALS with, for instance, mutations in *DCTN1*^{59,60} and *KIF5A*^{61,62}, highlighting functional connections of prioritized genes from the subthreshold loci with TDP-43 dysfunction and ALS. Future GWAS with larger sample sizes, potentially combining FTLD-TDP B and ALS, are required to firmly establish a genetic contribution of this pathway to disease.

Focusing on rare variants, exome-wide significant association with *TBK1* was observed in both FTLD-TDP A and B (but not FTLD-TDP C), confirming *TBK1* mutations as the most common cause of FTLD-TDP after *GRN* and *C9orf72*³. Novel genes with a significantly increased cumulative frequency of rare variants in specific FTLD-TDP subtypes as

compared to controls were also identified, and require confirmation in future studies. We acknowledge that limited sample sizes in these studies may have led to inflation and false positive findings; yet, this limitation is inherently linked to the unique and well-characterized study groups included in this study, the largest in the field of FTLD. We identified a significant association between rare variants in *C3ARI* and FTLD-TDP A. *C3ARI* plays a key role in the regulation of innate immunity and is involved in neuroinflammation^{63,64}. Interestingly, *Grn*^{-/-} mice present with upregulation of complement genes before onset of neurodegenerative features. Since *GRN* mutation carriers always present with FTLD-TDP A at autopsy, we suggest that aberrant activation of the complement pathway may play a major role in FTLD-TDP A pathology⁶⁵. We also identified a significant association between rare variants in *SMG8* and FTLD-TDP A. Homozygous pathogenic variants in the *SMG8* gene have been identified as a novel cause of autosomal recessive neurodevelopmental disorder⁶⁶. We further unveiled rare predicted pathogenic variants associated with FTLD-TDP B within *VIPRI*, which encodes for the vasoactive intestinal peptide (VIP) receptor 1. The variants are predicted to lead to an alteration of *VIPRI* function, impairing the VIP biological pathway. Indeed, *VIPRI* is activated upon binding by VIP, which exerts a neuroprotective effect mainly through glial cells^{67,68} even though neurons also express *VIPRs*^{69,70}. Notably, VIP is also a key regulator of innate and adaptive immunity⁷¹, making it an important therapeutic target for multiple neurodegenerative diseases. Altogether, our studies suggest that lysosome dysfunction and/or alterations in the innate and adaptive immune system are important contributors to both FTLD-TDP A and B risk, yet to varying degrees in each pathological subtype and with likely important variability in the contribution from each pathway among individual patients.

FTLD-TDP C was previously recognized as a clinicopathological entity distinct from FTLD-TDP A and B⁷², and our genetic studies support this notion, showing no overlap in common or rare risk genes with the other FTLD-TDP types. Importantly, however, while often considered a sporadic FTLD subtype^{14,73,74}, we implicate several genes and risk loci in FTLD-TDP C and uncover a potential role for mitochondrial membrane dysfunction and the notch signaling pathway. *C19orf52* (*TIMM29*), which mediates the import and insertion of multi-pass transmembrane proteins into the mitochondrial inner membrane, was identified as the first genome-wide significant risk locus for FTLD-TDP C. This locus was identified when svPPA patients were included in the GWAS, and both pathologically confirmed FTLD-TDP C and svPPA patients were found to contribute to the association (MAF FTLD-TDP C: 0.028, svPPA: 0.019, controls: 0.001; Supplementary Data 24). This finding illustrates the power we gained by including the clinically diagnosed patients, notwithstanding the fact that the pathological diagnosis will not be FTLD-TDP C in all. The inclusion of svPPA patients in our study is somewhat complicated by the evolving clinical definitions of patients affected by focal anterior temporal lobe (ATL) atrophy in recent years. Those with left-predominant ATL atrophy show severe anomia and verbal semantic deficits leading to diagnoses of svPPA and (previously) semantic dementia^{2,75}. However, patients with right ATL atrophy have been more challenging to fit into current diagnostic criteria and may have received diagnoses such as right-sided svPPA, right temporal variant of FTD, or, most recently, semantic behavioral variant of FTD^{76–81}. At the start of our study in 2019, this field was just starting to evolve, and we allowed inclusion of left- and right-sided svPPA patients as both were thought to have predominant FTLD-TDP C pathology⁸². More recently, through large cohort studies and the establishment of an international Working Group⁸³, systematic reassessment of clinically diagnosed patients with svPPA and bvFTD is ongoing with an emphasis on recognizing and diagnosing patients with right-temporal atrophy. As criteria are still in development and our clinical patients were not yet systematically assessed in this new framework, we also performed an additional GWAS including only

pathologically confirmed FTLD-TDP C patients (FTLD-TDP C*). This analysis led to the identification of 4 novel genome-wide significant loci (*LRP1B*, *COL22A1*, *TRPC4*, and *TMEM135*). While these loci remained nominally significant in the combined analysis, inspection of the results showed no contribution from the svPPA patients to the association (Supplementary Data 24). Even with a heterogeneous population of clinical patients, one would have expected an increased frequency of risk alleles in patients as compared to controls, raising concern that these additional loci may represent type I errors. In fact, the rare-variant burden analyzes in FTLD-TDP C also showed more hits when including the svPPA patients. First of all, we observed rare predicted pathogenic variants in *RBPJL*, which encodes for the recombination signal binding protein for immunoglobulin kappa J region like transcription factor. *RBPJL* can repress Notch target gene expression (*Hey1*, *Hey2*, *HeyL*, and *Notch3*)⁸⁴. As such, our findings align with a previous analysis of sub-genome-wide significant genes in clinical svPPA patients, which highlighted an overrepresentation of the Notch pathway⁸⁵. Interestingly, *RBPJL* and *L3MBTL1*, the second gene carrying rare predicted pathogenic variants in FTLD-TDP C, are part of the same co-expression module, suggesting that they are functionally related. Moreover, *L3MBTL1*, a histone methyl-lysine binding protein, is a key regulator of proteotoxicity associated with *C9orf72* dipeptide repeats and mutant *SOD1*⁸⁶ and was found to be increased in spinal cord of ALS patients. Furthermore, reduction of *L3MBTL1* expression in *Drosophila* models with the *C9orf72*-associated dipeptides poly(PR) or poly(GR) ameliorated the rough-eye phenotype⁸⁶, suggesting that loss of *L3MBTL1* expression is beneficial. While no RNA samples were accessible from rare variant carriers, nonsense-mediated decay escape has been reported in other genes linked to ALS⁸⁷. It is thus possible that the *L3MBTL1* variants lead to the generation of truncated proteins with toxic gain-of-function, but additional work is necessary to understand the disease etiology fully. Finally, rare variants in *ANO9* were also associated with FTLD-TDP C disease status. *ANO9* encodes for anocytamin 9, for which the biological function is currently unclear. *ANO9* was the only gene with exome-wide significance when svPPA patients were removed from the FTLD-TDP C subgroup.

When analyzed in sum, common variants associated with the different FTLD-TDP pathological subtypes appeared to be located in genes expressed in excitatory neurons, in contrast to AD risk variants, which are enriched in microglia. Interestingly, glutamatergic transmission impairment has been reported in FTLD^{88–92}, and voxel-based brain changes have been significantly associated with spatial distribution of mGluR5 in symptomatic *C9orf72* and *GRN* carriers⁹³. Therefore, and in line with previously reported studies, our data suggest that neurons are the major players in disease etiology, as compared to what has been observed in ADRD. Whether specific neuronal subpopulations differentially express associated genes could be the focus of future studies once single-nuclei transcriptomic datasets from FTLD-TDP patients and controls are available. Interestingly, the distribution of risk loci was specific to the cerebellar hemisphere and the frontal cortex for FTLD-TDP A, B, and C*, as opposed to FTLD-TDP C (with participants with svPPA), where genes expressed in small intestine were enriched in risk loci. While the link between gut microbiome and FTLD remains limited⁹⁴, our data suggest that the gut-brain axis might be of interest for future studies, especially in svPPA patients. In fact, emerging evidence also supports a role for the gut-brain axis in autoimmune diseases⁹⁵, a group of disorders that were found to be enriched in svPPA patients⁹⁶.

In prior studies, besides *UNC13A*, common variants in the *HLA* and *DPP6* loci, in *TMEM106B*, and most recently in *MAPT*, *APOE*, and *MOBP*, were reported to be associated with FTLD^{12,14,18}. The latter three loci and *HLA-DR5* locus were identified as associated with clinical FTLD and likely do not represent risk factors specific to TDP-43 dysfunction. *HLA-DQA2* and *DPP6* loci were reported as overall FTLD-TDP risk loci in phase I¹² but were not replicated in the current study. The relative

composition of patients with FTLD-TDP pathological subtypes in phase I and II (e.g., less FTLD-TDP A in phase II) and inclusion of clinically diagnosed individuals in phase II may have contributed to this; however, it is also possible that the increase in sample size reduced type I errors from phase I. Importantly, we identified and replicated in two independent cohorts the *UNC13A* and *TNIP1* loci associated with FTLD-TDP. Replication of the newly identified risk loci, each specific to distinct neuropathological FTLD-TDP subtypes, will require additional GWAS studies in the future. Obtaining sufficient samples will, however, be challenging, especially for FTLD-TDP A, which lacks a clear clinical correlate of the pathological phenotype. For FTLD-TDP C, the relative contribution of patients with left- and right-predominant ATL atrophy to the observed associations should be assessed once clinical criteria for patients with right temporal atrophy are finalized. Finally, functional characterization of the newly identified genes and loci may also provide mechanistic insight.

In conclusion, we confirmed *UNC13A* and identified 12 new genetic loci, i.e., *TNIP1*, *GRN*, *TINAG*, *MZT1*, *FARP2*, *RCL1*, *PSSSB*, *C19orf52*, *LRP1B*, *COL22A1*, *TMEM135*, and *TRPC4*, and 6 new genes with rare variants associated with FTLD-TDP risk, i.e., *C3ARI*, *SMG8*, *VIPRI*, *RBPJL*, *L3MBTL1*, and *ANO9*. Importantly, by enriching in neuropathologically confirmed patients and substantially increasing our cohort size, we uncovered distinct genetic aetiologies for each of the three main FTLD-TDP pathological subtypes. Our findings align with recent data obtained from cryo-electron microscopy, which identified distinct homomeric TDP-43 filaments in FTLD-TDP A and B and heteromeric amyloid filaments of ANXA11 and TDP-43 in FTLD-TDP C^{97–99}. The recognition of individual FTLD-TDP subtypes as potentially distinct diseases with unique pathomechanism may have important implications for the design of clinical trials and therapeutic interventions.

Methods

Ethics approval and consent to participate

This study was approved by the Mayo Clinic Institutional Review Board. All participants or their guardians provided written informed consent.

Samples

Our current dataset includes previously generated data through the International FTLD-TDP WGS consortium phase I² with 554 persons with clinicopathologically defined FTLD-TDP and newly generated phase II sequencing data from 32 FTLD-TDP A, 43 FTLD-TDP B, 66 FTLD-TDP C, 4 FTLD-TDP E, and 9 with unclassifiable FTLD-TDP pathology (abbreviated as FTLD-TDP U). To increase statistical power, we also sequenced 70 persons with clinical diagnosis of bvFTD/ALS, a clinical subtype associated with FTLD-TDP B, and 283 persons with svPPA, a clinical subtype associated with FTLD-TDP C. Overall, the total cohort pre-quality control was a combined FTLD-TDP cohort of 202 FTLD-TDP A, 237 FTLD-TDP B, 225 FTLD-TDP C, 4 FTLD-TDP D, 11 FTLD-TDP E, 29 FTLD-TDP U persons, 70 persons with bvFTD/ALS and 283 persons with svPPA (Table 1). After QC, 985 patients from 26 sites were included in the analysis (Supplementary Data 1 and Supplementary Data 25). Patients were diagnosed according to established diagnostic criteria^{1,2,75,100}; however, in the subgroup of patients with svPPA, in addition to including svPPA patients diagnosed according to Gorno-Tempini et al.², patients previously diagnosed with semantic dementia according to Neary et al.⁷⁵, and a few patients suspected to have the right temporal variant of FTD were included. For the latter group of patients, diagnostic criteria are only now being developed^{76,83}, we thus relied on the expert knowledge of the specialized dementia centers to identify these patients, recognizing the limitations of this approach, especially since this was not performed systematically in all contributing centers. All persons clinically or pathologically diagnosed with FTLD are referred to as patients throughout the manuscript. We further used WGS data from 982 participants from the Mayo Clinic

Biobank (from phase I),^{12,101} 322 new controls free of neurodegenerative disorder from Mayo Clinic with WGS available, and 2,037 controls derived from the ADSP. *C9orf72* repeat expansions were assessed in all patients using our previously reported two-step protocol, and Sanger sequencing was used to perform mutation analyses of *GRN*^{8,10}. Patients carrying repeat expansions in *C9orf72* or LOF mutations in *GRN*, both associated with autosomal dominant forms of FTLD-TDP, were removed prior to WGS. Study protocols were reviewed and approved by the appropriate institutional review boards.

Whole genome sequencing

In phase I of the International FTLD-TDP WGS consortium, WGS was generated on 554 patients with FTLD-TDP (512 passed QC in that study)¹². Briefly, whole blood- or brain-derived DNA from 499 unrelated FTLD-TDP patients and 982 participants from the Mayo Clinic Biobank Study were sequenced at HudsonAlpha using the standard library preparation protocol using the NEBNext[®] DNA Library Prep Master Mix Set for Illumina[®] (New England BioLabs Inc., Ipswich, MA, USA). Concentration of the libraries was assessed by Qubit[®] 2.0 Fluorometer, and the quality of the libraries was estimated by a DNA 5 K chip on a Caliper GX. Accurate quantification was determined using the qPCR-based KAPA Biosystems Library Quantification kit (Kapa Biosystems, Inc., Woburn, MA, USA). Each sample was sequenced on one lane of Illumina's HiSeq X instrument using v2 flow cells and reagents to target 30× genomic coverage. Fastq files previously generated on an Illumina HiSeq X for 55 FTLD-TDP patients were obtained from 3 sites: UCSF (*n* = 36), DZNE (*n* = 14), and NSW (*n* = 5).

In phase II, additional WGS of 507 patients with FTLD-TDP, svPPA, bvFTD/ALS, and 322 controls free of neurodegenerative disorders was performed at USUHS sequencing center or Mayo Clinic Rochester using the TruSeq DNA PCR-Free Library preparation Kit (Illumina), followed by Whole Genome Sequencing by synthesis (SBS) chemistry on HiSeq X Illumina platform using the HiSeq X Ten Reag. kit v2.5. Fastq files for all patients and controls were transferred to Mayo Clinic and processed through the Mayo Genome GPS v4.0 pipeline in batches of up to 75 samples using the Burrows–Wheeler Aligner to map reads to the human reference sequence (GRCh38 build). Local realignment around indels and variant calling were performed using Genome Analysis Toolkit (GATK) HaplotypeCaller, followed by variant recalibration (VQSR) according to GATK best practice recommendations. Participants from the Mayo Clinic Biobank with a possible clinical diagnosis or family history of a neurodegenerative disorder were removed during analysis.

To enhance our study, we incorporated genomic variant call format (gVCF) files from 2037 controls obtained from the Alzheimer's Disease Sequencing Project (ADSP). gVCF files provide a comprehensive record of variant calls and reference positions, which are essential for accurate joint-genotyping. The gVCF files from ADSP controls were merged with our cohort's gVCF files using the joint-genotyping approach implemented with the GATK. By merging these gVCFs, we ensured all our patients and controls were analyzed together, allowing for a more robust comparison and reducing batch effects. Overall, we obtained genomic data on a total of 1061 patients and 3341 controls.

Sample-level quality control and definition of subgroups

Samples with less than 30× coverage in more than 50% of the genome, call rate below 85%, sex error, and contamination defined by a FREEMIX score above 0.04 (4% or more of non-reference bases are observed in reference sites) were removed. In more detail, estimates of sample contamination were calculated using data on all autosomes with 1000 Genomes European array allele frequencies as reference. The estimated contamination value, FREEMIX 1.3, provides a sequence-only estimate of contamination on a 0–1 scale using excessive heterozygosity. In addition, we identified 31 non-European White participants (Admixture EUR Probability <0.7), which we removed from

analysis because of the small sample size and to increase genetic background homogeneity. Information from chromosomes X and Y was used to estimate sex. All SNVs having MAF > 0.05, variant call rate > 0.80, Hardy Weinberg Equilibrium p value > $1e-8$, and LD r^2 < 0.8 were used for these calculations. Samples whose reported sex did not match the estimated sex based on genomic data using the check-sex PLINK command were removed. At this step, joint genotyping on all samples was performed. A final relatedness measurement was calculated using PREST¹⁰², and duplicates were removed, while only one individual per family was kept. In total, 985 pathologically confirmed FTLD-TDP or presumed FTLD-TDP patients clinically presenting with svPPA or bvFTD/ALS, as well as 3153 neurologically normal controls passed all QC measures (Supplementary Data 25). Age at onset of svPPA and bvFTD/ALS did not differ from the age at onset of FTLD-TDP C ($P=1$) and FTLD-TDP B patients ($P=1$), respectively. Based on these findings and the previously established associations between the svPPA and bvFTD/ALS clinical diagnoses with specific FTLD-TDP pathological subtypes, we combined svPPA with FTLD-TDP C and bvFTD/ALS with FTLD-TDP B patients in all analyzes (except where explicitly specified, such as in FTLD-TDP C* analyzes). Within our overall cohort of 193 FTLD-TDP A, 288 FTLD-TDP B (defined as FTLD-TDP B and bvFTD/ALS) and 467 FTLD-TDP C (defined as FTLD-TDP C and svPPA), the ages at onset and death differed significantly between the pathological FTLD-TDP subtypes (Table 1 and Supplementary Fig. 11). FTLD-TDP A patients had a later age at onset than FTLD-TDP B and FTLD-TDP C groups ($P=4.73 \times 10^{-8}$, $P=1.37 \times 10^{-13}$, respectively), and a later age at death ($P=4.00 \times 10^{-15}$, $P=3.00 \times 10^{-6}$, respectively). FTLD-TDP B had an earlier age at death as compared to FTLD-TDP C ($P=5.60 \times 10^{-8}$). Differences in age distribution between patient groups were assessed using the Kruskal–Wallis test followed by Wilcoxon test, correcting for multiple testing. Corrected Bonferroni P values are provided.

Variant level quality control

Genotype calls with genotype quality < 20 and/or depth (DP) < 10 were set to missing, and variants with edit-distance > 4 and call rate < 80% were removed from all subsequent analyzes, leading to a total of 85,345,466 variants. For all analyzes, only variants that pass VQSR (127,658 variants removed) and with a call rate > 95% in patients and controls were considered (591,431 variants removed). Functional annotation of variants was performed using ANNOVAR (version 2016Feb01). Rare loss-of-function variants frameshift insertion/deletion/block substitution, stopgain, stoploss, and splicing single-nucleotide variants (SNVs) and missense with REVEL score > 0.75²² identified in exome-wide significantly associated genes (Supplementary Data 18–23) were confirmed in patients by Sanger sequencing (primers available upon request). For the known neurodegenerative disease genes (*GRN*, *MAPT*, *TBK1*, *OPTN*, *VCP*, *TARDBP*, *CHCHD10*, *SQSTM1*, *UBQLN2*, *hnRNPA1*, *hnRNPA2B1*, *CSF1R*, *FUS*, *CHMP2B*, and *LRRK2*), potentially pathogenic rare variants were also identified and confirmed by Sanger sequencing ($n=25$ and Supplementary Data 26).

Generation of principal components

Prior to running genetic association analyzes, principal component (PC) analysis was performed using a subset of variants meeting the following criteria: minor allele frequency (MAF) > 5% and full sample Hardy-Weinberg Equilibrium (HWE) $P>1 \times 10^{-5}$. Influential regions such as the *HLA* region were removed, and variants were pruned by LD with r^2 threshold of 0.1 prior to PC analysis. This analysis identified that the 13 top PCs were significantly associated with patient/control status.

Variant-level analysis of common variants

For the common variant GWAS, SNV with MAF > 0.01 in patients or controls ($n=7,178,250$ variants), and HWE $P>1.00 \times 10^{-6}$ in controls were analyzed (17,450 variants removed). In addition, since whole

genome sequencing of FTLD-TDP patients and controls was performed at multiple sites, a test was performed to identify variants with significant differences in genotype distributions between sequencing batches, and 592,701 SNVs showing evidence of batch effects ($p<0.05$) were removed, leading to a total of 6,568,099 variants analyzed.

For all remaining variants, association of genotypes with the patient/control status was assessed using logistic regression with allele dosage as the predictor, assuming log-additive allele effects. Genome-wide significance was defined as $P<5 \times 10^{-8}$. Sex and the first 13 PCs were included as covariates in the models. The SNV-level analyzes were performed using PLINKv.00a23LM2, combining all FTLD-TDP patients (FTLD-TDP All) and in FTLD-TDP pathological subtypes. MAGMA (v1.6) was used to perform gene-based analysis of common variants using summary statistics. MAGMA is a tool designed to analyze associations at the gene level by aggregating SNV p values while accounting for LD. Dementia-seq vcf was processed the exact same way as our data, except that 10 PCs were included in the model to perform common variant association analysis. Identification of duplicate samples between our discovery dataset and the Dementia-seq data was performed, and all duplicates were removed. Meta-analyzes of FTLD-TDP phase II with publicly available datasets from the Dementia-seq project (phs001963.v2.pl) were performed under a fixed-effects model comparing our data with 2102 FTLD patients and 1748 controls from the Dementia-seq project using Metal¹⁰³.

Colocalization analyzes

We performed colocalization analysis for *UNC13A* and *TNIP1* loci (top SNVs ± 100 kb) with ALS (GCST90027164) and ADRD (GCST90027158) using the “coloc” package version 4.0.4 in *R* using our meta-analyzes data. When the summary statistics of the other trait were expressed on another build than GRCh38, the variant alleles and positions were converted. We set the prior probabilities to $\pi_1=1 \times 10^{-4}$, $\pi_2=1 \times 10^{-4}$, and $\pi_{12}=1 \times 10^{-5}$ for a causal variant in trait 1 or trait 2 and a shared causal variant between traits 1 and 2, respectively (default parameters). Sensitivity analysis was performed at $\pi_{12}=1 \times 10^{-6}$. $P<0.05$ was considered statistically significant.

Tissue and cell type enrichment analysis

Tissue and cell type enrichment analyzes were performed using the summary statistics (variants with $P<10^{-5}$) and FUMA¹⁰⁴. Briefly, FUMA aggregates summary statistics per gene to calculate gene-wise association signals using MAGMA version 1.6 and subsequently tests whether tissues and cell types are enriched for expression of these genes. For tissue enrichment analysis, we used the GTEx version 8 reference set. $P<0.05$ across all tissues ($n=54$) was considered statistically significant. For cell type enrichment analyzes, we used human-derived single-cell RNA-seq data from major brain cell types (PsychENCODE). Excitatory and inhibitory neurons from the PsychENCODE dataset were labeled based on their transcriptional profile from 1 to 8¹⁰⁵. $P<0.05$ was considered statistically significant.

Gene prioritization and functional interpretation of GWAS

We performed the gene prioritization and functional interpretation analyzes for FTLD-TDP All and each FTLD-TDP pathological subtype separately by using the subtype-specific GWAS summary statistics on all variants. We adapted a systematic gene prioritization and functional interpretation strategy (as previously described in Bellenguez et al.¹⁹) to prioritize GWAS-implicated candidate risk genes and nominate possible downstream biological mechanisms. Briefly, six distinct domains, that are related to lead variant annotation and molecular QTL-GWAS integration analyzes (e.g., colocalization and TWAS) in FTLD-relevant tissues and cell types were systematically assessed: (1) variant annotation, (2) eQTL-GWAS integration, (3) sQTL-GWAS integration, (4) protein expression QTL (pQTL)-GWAS integration, (5)

mQTL-GWAS integration, and (6) histone acetylation QTL (haQTL)-GWAS integration; for which detailed information on categories and subcategories is provided in Supplementary Data 3.

In the variant annotation domain, for each lead variant at each locus, we queried which candidate risk genes were the nearest protein-coding genes with respect to the genomic position of the lead variants, and/or whether the lead variant was a rare (MAF < 1% in gnomAD v4 non-Finnish European samples) and/or protein-altering (missense or predicted LOF) variant for the same nearest protein-coding genes. In the molecular QTL-GWAS integration domains, we leveraged molecular cis-QTL catalogs for different molecular phenotypes (i.e., gene expression, splicing, protein expression, methylation, and histone acetylation) in FTLD-relevant tissues and cell types, we performed genetic colocalization analyzes between molecular cis-QTL and GWAS signals, TWAS, and proteome-wide association studies (PWAS). For these analyzes, we processed and used publicly available molecular QTL catalogs; namely, FTLD-relevant bulk brain regions from AMP-AD^{106–109} (as reanalyzed in Bellenguez et al.¹⁹) and GTEx v8¹¹⁰ cohorts for the bulk brain eQTLs and sQTLs, eight major brain cell types (excitatory neurons, inhibitory neurons, astrocytes, oligodendrocytes, microglia, oligodendrocyte precursor cells/committed oligodendrocyte precursors [OPCs/COPs], pericytes, and endothelial cells) from Bryois et al.¹¹¹ and primary microglia from Young et al.¹¹² and the MiGA study¹¹³ for the brain cell-type-specific eQTLs (ct-eQTL) and for microglia sQTLs (from the MiGA study), dorsolateral prefrontal cortex (DLPFC) pQTLs from Wingo et al.¹¹⁴ (v2), and DLPFC mQTLs and haQTLs from Brain xQTL serve (June 2021 release)^{114,115}. Finally, we also included naïve state monocyte and macrophage eQTL catalogs^{116–121} reanalyzed by eQTL Catalog (Release 6)¹²² and lymphoblastoid cell line (LCL) eQTLs from GTEx v8¹¹⁰ and the European Alzheimer & Dementia Biobank (EADB) Belgian LCL cohorts¹⁹. Using each of these molecular QTL catalogs, we first investigated whether the reported lead variants in this study were significant molecular QTLs for the quantified levels of molecular phenotypes in tissues and cell types of interest. Moreover, for each quantified molecular phenotype in these catalogs, we performed molecular QTL-GWAS coloc (v5.2.2) analyzes to determine if specific molecular QTL signals are colocalized (at coloc PP4 ≥ 70%) with FTLD subtype GWAS signals. Of note, for mQTL-GWAS integrative analyzes, the CpGs were assigned to genes using BECon annotations¹²³ whenever available, and if not, the CpGs were mapped to the nearest genes based on GENCODE v24; while for haQTL-GWAS integrative analyzes, the histone acetylation peaks were assigned to the nearest genes based on GENCODE v24 as well. Finally, we conducted TWAS (using FUSION and S-PrediXcan [implemented in MetaXcan] tools) for each heritable feature modeled in gene expression (eTWAS; followed by eTWAS fine mapping with FOCUS¹²⁴ [v0.803] within 1 Mb extended genome-wide significant lead variant genetic regions in each FTLD-TDP subtype GWAS), splicing (sTWAS), and PWAS reference panels derived from AMP-AD bulk brain^{106–109}, GTEx bulk brain and LCL¹¹⁰, EADB Belgian LCL¹⁹, and Wingo et al. DLPFC data¹¹⁴, to identify the significant associations (after Bonferroni correction) between predicted levels of gene expression, splicing, and protein expression with each FTLD subtype-specific genetic risk. Detailed description and details (e.g., number of samples, significance criteria, references, and sources) of these molecular QTL catalogs used in this study for the systematic gene prioritization strategy and functional interpretation of FTLD-TDP GWAS results can be found in Supplementary Data 5.

Using a predetermined weighting scheme for each type of evidence (see Supplementary Data 3), we computed a gene prioritization score (between 0 and 87) for each gene, which was constructed by the weighted sum of the hits in different subcategories within six distinct domains described above. As described in Bellenguez et al.¹⁹ in detail, we gave higher weights for the hits obtained through the brain QTLs rather than other tissue QTLs, for the replicated hits across multiple

catalogs or reference panels, and for the fine-mapped eTWAS hits. After obtaining weighted gene prioritization scores in each FTLD-TDP subtype-specific gene prioritization analysis, we first assigned each candidate risk gene (with gene prioritization score > 0) to the genome-wide significant loci if their gene coordinates (based on GENCODE v24) are positioned within a ± 1 Mb window of the identified lead variants (Table 2). The rest of the candidate risk genes in subthreshold regions (nominated by Coloc and TWAS analyzes only) were grouped together if they were positioned together (< 1 Mb), and these subthreshold regions were indexed and named as subthreshold loci. The candidate risk genes in genome-wide significant and subthreshold loci were also annotated by the evidence of minimum *P* observed within 1 Mb of the gene coordinates in related FTLD-TDP subtype-specific GWAS summary statistics. We then ranked the protein-coding genes per locus in each FTLD subtype-specific analysis based on their total weighted scores, and investigated the relative score differences between the highest-ranked protein-coding gene and the other candidate risk genes in each locus, together with the overall total weighted score of the top-ranked gene. We then classified candidate risk genes in each locus as tier 1 and tier 2 prioritized risk genes, respectively having a higher and lower level of confidence for being a true risk gene in a given locus (see Bellenguez et al.¹⁹ for detailed description). As also described in Bellenguez et al.¹⁹, the gene prioritization pipeline determines a single tier 1 prioritized risk gene in each locus if there is adequate evidence, meanwhile additional tier 2 prioritized risk genes in the same loci or multiple tier 2 prioritized risk genes in a locus can also be assigned based on the score distribution of candidate genes in the investigated loci.

Gene ontology analyzes

GO on tier 1 genes identified in FTLD-TDP All or in individual FTLD-TDP subtype analyzes were performed using an R package, which aggregates summary statistics and assesses GO term enrichment. GO terms were collapsed using the RVizgo R package. Only terms with two or more genes were considered in the analyzes. *P* < 0.05 was considered statistically significant.

Genetic correlation analyzes

We assessed genetic similarity between FTLD-TDP All and ALS and ADRD using the LD score regression (LDSC, <https://github.com/bulik/ldsc>). We estimated genetic correlations attributable to genome-wide SNPs (r_g) between FTLD-TDP All and ALS, and FTLD-TDP All and ADRD using the default settings in the LDSC software and pre-calculated LD scores from the 1000 Genomes European reference population, supplied with the LDSC software.

Gene-level analysis of rare variants

Association of rare variants with the patient/control status was assessed using an unweighted burden test implemented using the SKAT_1.2.1R package. Only VQSR-pass variants with call rate > 90%, ED ≤ 4, and MAF < 0.01 in either patients or controls were included. We included only frameshift (insertion/deletion/block substitution), stopgain, stoploss, and splicing SNVs (jointly defined as LOF variants), and non-synonymous SNVs with REVEL score above 0.75²². Only genes with at least 3 patients carrying rare variants were retained. Sex and the first thirteen PCs were used as covariates. Exome-wide significance with *p* value < 2.5 × 10⁻⁶ (Bonferroni correction for 20,000 genes) was used. The rare variants in the top genes were confirmed by Sanger sequencing in all patient samples and visually inspected to eliminate sequencing errors. One gene enriched in rare variants in FTLD-TDP A (*TDRD5*) as compared to controls failed at the inspection stage due to the inclusion of a multi-allelic variant around the repetitive C-terminal end of the gene, which could not be definitively confirmed. Rare variants enriched in two genes in FTLD-TDP C (*C4orf47* and *TYRO3*) failed confirmation via Sanger sequencing.

RBPJL and L3MBTL1 RNA expression

Assessment of module membership of *RBPJL* and *L3MBTL1* was performed using the gene co-expression analysis from the BrainEXP-NPD²³ website using default parameters. Single-nuclei RNA expression was assessed using the transcriptomic comparative viewer of the Seattle Alzheimer's Disease Brain cell Atlas from middle temporal gyrus of 84 aged donors (42 cognitively normal and 42 with dementia).

Reporting summary

Further information on research design is available in the Nature Portfolio Reporting Summary linked to this article.

Data availability

The processed (summary statistics) data generated in this study have been deposited in the GWAS catalog database under accession codes GCP001210 (GCST90558311, GCST90558312, GCST90558313, and GCST90558314) [https://ftp.ebi.ac.uk/pub/databases/gwas/summary_statistics/]. Whole genome sequencing data from the 507 FTLT-DTP patients and 322 controls generated in Phase II are available as follows: raw sequencing data and VCF for 435 FTLT-DTP patients and 19 control individuals have been deposited in the dbGAP platform as part of the dataset with accession code phs003309 [https://www.ncbi.nlm.nih.gov/projects/gap/cgi-bin/study.cgi?study_id=phs003309.v1.p1]. For the 435 FTLT-DTP patients, access is restricted: 271 can be for General Research Use, 1 is for Health/Medical/Biomedical research only, and 163 are for 'Disease-Specific (Neurodegenerative Disorders)' research only. The 19 controls can also be used for Disease-Specific (Neurodegenerative Disorders) research only. Access can be obtained by applying for dbGaP Authorized Access via <https://view.ncbi.nlm.nih.gov/dbgap-controlled>. The gVCF genetic data from ADSP used in Phase II are available through restricted to not-for-profit organizations, access can be obtained by applying at <https://dss.niagads.org/>. The genetic data for Phase I participants¹² and the remaining 72 FTLT-DTP patients and 303 controls from Phase II are not part of dbGAP accession phs003309 and are not available due to data sharing constraints related to the participants' consent form. From the Phase II post quality control dataset, 303 controls from Mayo Clinic, USA, and 51 FTLT-DTP patients could not be shared (48 from Erasmus Medical Center, The Netherlands, 1 from Mayo Clinic, USA, 1 from Indiana University, USA, and 1 from University of California, San Francisco). The PsychENCODE data used in this study are publicly available through the FUMA platform [<https://fuma.ctglab.nl/>]. Dataset and molecular QTLs used in the gene prioritization are publicly available (see also Supplementary Data 5): The eQTLs and eTAS reference panels in AD-relevant bulk brain regions from AMP-AD cohorts and in LCLs from the EADB Belgian cohort, as analyzed by Bellenguez et al.¹⁹ are publicly available in the Zenodo database under accession code [5745927](https://zenodo.org/record/5745927). The sQTLs and sTAS reference panels used in this study from AD-relevant bulk brain regions from AMP-AD cohorts and from LCLs from the EADB Belgian cohort, as analyzed by Bellenguez et al.¹⁹ are publicly available in the Zenodo database under accession code [5745929](https://zenodo.org/record/5745929). The Bryois et al.¹¹¹ ct-eQTL catalogs used in this study are publicly available in the Zenodo database under accession code [5543734](https://zenodo.org/record/5543734). The eQTL data used in this study are publicly available in the eQTL catalog database [<https://www.ebi.ac.uk/eQTL/>]. The mQTL and haQTL catalogs used in this study are publicly available in the Brain xQTL Serve database [<https://mostafavilab.stat.ubc.ca/xqtl/>] issued from Ng et al.¹¹⁵. The eQTL and sQTL catalogs used in this study are available in the GTEx v8 database [<https://www.gtexportal.org/>]. The GTEx v8 expression and splicing prediction models for eTAS/sTAS used in this study are available at <https://predictdb.org/post/2021/07/21/gtex-v8-models-on-eqtl-and-sqtl/#mashr-based-models>. The microglial eQTL data used in this study are available in the Zenodo database under accession code [4118605](https://zenodo.org/record/4118605). The microglial sQTL data used in this study are available in the Zenodo database under accession code [4118403](https://zenodo.org/record/4118403). The microglial

meta-analysis data used in this study are available in the Zenodo database under accession code [4118676](https://zenodo.org/record/4118676). The pQTL v2 data used in this study is available in the Synapse database under accession code [syn23627957](https://www.synapse.org/#!Synapse:syn23627957) [<https://www.synapse.org/#!Synapse:syn23627957>], from the publication Wingo et al.¹¹⁴. The BECon annotations used in this study are available at <https://redgar598.shinyapps.io/BECon/>.

References

- Rascovsky, K. et al. Sensitivity of revised diagnostic criteria for the behavioural variant of frontotemporal dementia. *Brain* **134**, 2456–2477 (2011).
- Gorno-Tempini, M. L. et al. Classification of primary progressive aphasia and its variants. *Neurology* **76**, 1006–1014 (2011).
- Lee, E. B. et al. Expansion of the classification of FTLT-DTP: distinct pathology associated with rapidly progressive frontotemporal degeneration. *Acta Neuropathol.* **134**, 65–78 (2017).
- Mackenzie, I. R. et al. A harmonized classification system for FTLT-DTP pathology. *Acta Neuropathol.* **122**, 111–113 (2011).
- Chatterjee, M. et al. Plasma extracellular vesicle tau and TDP-43 as diagnostic biomarkers in FTD and ALS. *Nat. Med.* **30**, 1771–1783 (2024).
- Mackenzie, I. R. et al. Heterogeneity of ubiquitin pathology in frontotemporal lobar degeneration: classification and relation to clinical phenotype. *Acta Neuropathol.* **112**, 539–549 (2006).
- Mackenzie, I. R. & Neumann, M. Reappraisal of TDP-43 pathology in FTLT-U subtypes. *Acta Neuropathol.* **134**, 79–96 (2017).
- Baker, M. et al. Mutations in progranulin cause tau-negative frontotemporal dementia linked to chromosome 17. *Nature* **442**, 916–919 (2006).
- Cruts, M. et al. Null mutations in progranulin cause ubiquitin-positive frontotemporal dementia linked to chromosome 17q21. *Nature* **442**, 920–924 (2006).
- DeJesus-Hernandez, M. et al. Expanded GGGGCC hexanucleotide repeat in noncoding region of C9ORF72 causes chromosome 9p-linked FTD and ALS. *Neuron* **72**, 245–256 (2011).
- Renton, A. E. et al. A hexanucleotide repeat expansion in C9ORF72 is the cause of chromosome 9p21-linked ALS-FTD. *Neuron* **72**, 257–268 (2011).
- Pottier, C. et al. Genome-wide analyses as part of the international FTLT-DTP whole-genome sequencing consortium reveals novel disease risk factors and increases support for immune dysfunction in FTLT. *Acta Neuropathol.* **137**, 879–899 (2019).
- Pottier, C. et al. Whole-genome sequencing reveals important role for TBK1 and OPTN mutations in frontotemporal lobar degeneration without motor neuron disease. *Acta Neuropathol.* **130**, 77–92 (2015).
- Ferrari, R. et al. Frontotemporal dementia and its subtypes: a genome-wide association study. *Lancet Neurol.* **13**, 686–699 (2014).
- Mackenzie, I. R. et al. The neuropathology of frontotemporal lobar degeneration caused by mutations in the progranulin gene. *Brain* **129**, 3081–3090 (2006).
- Mackenzie, I. R. & Neumann, M. Subcortical TDP-43 pathology patterns validate cortical FTLT-DTP subtypes and demonstrate unique aspects of C9orf72 mutation cases. *Acta Neuropathol.* **139**, 83–98 (2020).
- Van Deerlin, V. M. et al. Common variants at 7p21 are associated with frontotemporal lobar degeneration with TDP-43 inclusions. *Nat. Genet.* **42**, 234–239 (2010).
- Manzoni, C. et al. Genome-wide analyses reveal a potential role for the MAPT, MOBP, and APOE loci in sporadic frontotemporal dementia. *Am. J. Hum. Genet.* **111**, 1316–1329 (2024).
- Bellenguez, C. et al. New insights into the genetic etiology of Alzheimer's disease and related dementias. *Nat. Genet.* **54**, 412–436 (2022).

20. Project Min, E.A.L.S.S.C. Project MinE: study design and pilot analyses of a large-scale whole-genome sequencing study in amyotrophic lateral sclerosis. *Eur. J. Hum. Genet.* **26**, 1537–1546 (2018).
21. Benyamin, B. et al. Cross-ethnic meta-analysis identifies association of the GPX3-TNIP1 locus with amyotrophic lateral sclerosis. *Nat. Commun.* **8**, 611 (2017).
22. Ioannidis, N. M. et al. REVEL: an ensemble method for predicting the pathogenicity of rare missense variants. *Am. J. Hum. Genet.* **99**, 877–885 (2016).
23. Jiao, C. et al. BrainEXP: a database featuring with spatiotemporal expression variations and co-expression organizations in human brains. *Bioinformatics* **35**, 172–174 (2019).
24. van Es, M. A. et al. Genome-wide association study identifies 19p13.3 (UNC13A) and 9p21.2 as susceptibility loci for sporadic amyotrophic lateral sclerosis. *Nat. Genet.* **41**, 1083–1087 (2009).
25. Placek, K. et al. UNC13A polymorphism contributes to frontotemporal disease in sporadic amyotrophic lateral sclerosis. *Neurobiol. Aging* **73**, 190–199 (2019).
26. Brown, A. L. et al. TDP-43 loss and ALS-risk SNPs drive mis-splicing and depletion of UNC13A. *Nature* **603**, 131–137 (2022).
27. Ma, X. R. et al. TDP-43 represses cryptic exon inclusion in the FTD-ALS gene UNC13A. *Nature* **603**, 124–130 (2022).
28. Augustin, I., Rosenmund, C., Sudhof, T. C. & Brose, N. Munc13-1 is essential for fusion competence of glutamatergic synaptic vesicles. *Nature* **400**, 457–461 (1999).
29. Restuadi, R. et al. Functional characterisation of the amyotrophic lateral sclerosis risk locus GPX3/TNIP1. *Genome Med.* **14**, 7 (2022).
30. Tanaka, H. et al. ITIH4 and Gpx3 are potential biomarkers for amyotrophic lateral sclerosis. *J. Neurol.* **260**, 1782–1797 (2013).
31. Wainberg, M., Andrews, S. J. & Tripathy, S. J. Shared genetic risk loci between Alzheimer’s disease and related dementias, Parkinson’s disease, and amyotrophic lateral sclerosis. *Alzheimers Res. Ther.* **15**, 113 (2023).
32. Oshima, S. et al. ABIN-1 is a ubiquitin sensor that restricts cell death and sustains embryonic development. *Nature* **457**, 906–909 (2009).
33. Su, Z. et al. ABIN-1 heterozygosity sensitizes to innate immune response in both RIPK1-dependent and RIPK1-independent manner. *Cell Death Differ.* **26**, 1077–1088 (2019).
34. Zhou, J. et al. A20-binding inhibitor of NF-kappaB (ABIN1) controls Toll-like receptor-mediated CCAAT/enhancer-binding protein beta activation and protects from inflammatory disease. *Proc. Natl. Acad. Sci. USA* **108**, E998–E1006 (2011).
35. Shade, L. M. P. et al. GWAS of multiple neuropathology endophenotypes identifies new risk loci and provides insights into the genetic risk of dementia. *Nat. Genet.* **56**, 2407–2421 (2024).
36. Lee, Y. et al. Coordinate regulation of the senescent state by selective autophagy. *Dev. Cell* **56**, 1512–1525 e7 (2021).
37. Freischmidt, A. et al. Haploinsufficiency of TBK1 causes familial ALS and fronto-temporal dementia. *Nat. Neurosci.* **18**, 631–636 (2015).
38. Katsumata, Y. et al. Multiple gene variants linked to Alzheimer’s-type clinical dementia via GWAS are also associated with non-Alzheimer’s neuropathologic entities. *Neurobiol. Dis.* **174**, 105880 (2022).
39. Katsumata, Y., Nelson, P. T., Ellingson, S. R. & Fardo, D. W. Gene-based association study of genes linked to hippocampal sclerosis of aging neuropathology: GRN, TMEM106B, ABCC9, and KCNMB2. *Neurobiol. Aging* **53**, 193 e17–193 e25 (2017).
40. Nelson, P. T. et al. Limbic-predominant age-related TDP-43 encephalopathy (LATE): consensus working group report. *Brain* **142**, 1503–1527 (2019).
41. Josephs, K. A. et al. Pathological, imaging and genetic characteristics support the existence of distinct TDP-43 types in non-FTLD brains. *Acta Neuropathol.* **137**, 227–238 (2019).
42. Vicente, T. C. et al. C-terminal TMEM106B fragments in human brain correlate with disease-associated TMEM106B haplotypes. *Brain* **146**, 4055–4064 (2023).
43. Swift, I. J. et al. A systematic review of progranulin concentrations in biofluids in over 7000 people-assessing the pathogenicity of GRN mutations and other influencing factors. *Alzheimers Res. Ther.* **16**, 66 (2024).
44. Nicholson, A. M. et al. Progranulin protein levels are differently regulated in plasma and CSF. *Neurology* **82**, 1871–1878 (2014).
45. Hook, V. et al. Cathepsin B in neurodegeneration of Alzheimer’s disease, traumatic brain injury, and related brain disorders. *Biochim. Biophys. Acta Proteins Proteomics* **1868**, 140428 (2020).
46. Lee, C. W. et al. The lysosomal protein cathepsin L is a progranulin protease. *Mol. Neurodegener.* **12**, 55 (2017).
47. Zhou, X. et al. Lysosomal processing of progranulin. *Mol. Neurodegener.* **12**, 62 (2017).
48. Vesa, J. et al. Mutations in the palmitoyl protein thioesterase gene causing infantile neuronal ceroid lipofuscinosis. *Nature* **376**, 584–587 (1995).
49. Camp, L. A., Verkruyse, L. A., Afendis, S. J., Slaughter, C. A. & Hofmann, S. L. Molecular cloning and expression of palmitoyl-protein thioesterase. *J. Biol. Chem.* **269**, 23212–23219 (1994).
50. Branchu, J. et al. Loss of spatascin function alters lysosomal lipid clearance leading to upper and lower motor neuron degeneration. *Neurobiol. Dis.* **102**, 21–37 (2017).
51. Han, S. M. et al. VAPB/ALS8 MSP ligands regulate striated muscle energy metabolism critical for adult survival in caenorhabditis elegans. *PLoS Genet.* **9**, e1003738 (2013).
52. Cingolani, F. & Czaja, M. J. Regulation and functions of autophagic lipolysis. *Trends Endocrinol. Metab.* **27**, 696–705 (2016).
53. Liu, Y. et al. A C9orf72-CARM1 axis regulates lipid metabolism under glucose starvation-induced nutrient stress. *Genes Dev.* **32**, 1380–1397 (2018).
54. Conibear, E. & Stevens, T. H. Vps52p, Vps53p, and Vps54p form a novel multisubunit complex required for protein sorting at the yeast late Golgi. *Mol. Biol. Cell* **11**, 305–323 (2000).
55. Liewen, H. et al. Characterization of the human GARP (Golgi associated retrograde protein) complex. *Exp. Cell Res.* **306**, 24–34 (2005).
56. Wei, J. et al. The GARP complex is involved in intracellular cholesterol transport via targeting NPC2 to lysosomes. *Cell Rep.* **19**, 2823–2835 (2017).
57. Guise, A. J. et al. TDP-43-stratified single-cell proteomics of post-mortem human spinal motor neurons reveals protein dynamics in amyotrophic lateral sclerosis. *Cell Rep.* **43**, 113636 (2024).
58. Yoshimura, S., Gerondopoulos, A., Linford, A., Rigden, D. J. & Barr, F. A. Family-wide characterization of the DENN domain Rab GDP-GTP exchange factors. *J. Cell Biol.* **191**, 367–381 (2010).
59. Deshimaru, M. et al. DCTN1 binds to TDP-43 and regulates TDP-43 aggregation. *Int. J. Mol. Sci.* **22**, 3985 (2021).
60. He, J., Yu, W., Liu, X. & Fan, D. An identical DCTN1 mutation in two Chinese siblings manifest as dHMN and ALS respectively: a case report. *Amyotroph. Lateral Scler. Frontotemporal Degener.* **23**, 149–153 (2022).
61. Nicolas, A. et al. Genome-wide analyses identify KIF5A as a Novel ALS gene. *Neuron* **97**, 1267–1288 (2018).
62. Xia, C. H. et al. Abnormal neurofilament transport caused by targeted disruption of neuronal kinesin heavy chain KIF5A. *J. Cell Biol.* **161**, 55–66 (2003).
63. Litvinchuk, A. et al. Complement C3aR inactivation attenuates tau pathology and reverses an immune network deregulated in tauopathy models and Alzheimer’s disease. *Neuron* **100**, 1337–1353 e5 (2018).
64. Veerhuis, R., Nielsen, H. M. & Tenner, A. J. Complement in the brain. *Mol. Immunol.* **48**, 1592–1603 (2011).

65. Kao, A. W., McKay, A., Singh, P. P., Brunet, A. & Huang, E. J. Progranulin, lysosomal regulation and neurodegenerative disease. *Nat. Rev. Neurosci.* **18**, 325–333 (2017).
66. Alzahrani, F. et al. Recessive, deleterious variants in SMG8 expand the role of nonsense-mediated decay in developmental disorders in humans. *Am. J. Hum. Genet.* **107**, 1178–1185 (2020).
67. Brenneman, D. E., Hauser, J., Spong, C. Y. & Phillips, T. M. Chemokines released from astroglia by vasoactive intestinal peptide. Mechanism of neuroprotection from HIV envelope protein toxicity. *Ann. NY Acad. Sci.* **921**, 109–114 (2000).
68. Brenneman, D. E. et al. Vasoactive intestinal peptide. Link between electrical activity and glia-mediated neurotrophism. *Ann. NY Acad. Sci.* **897**, 17–26 (1999).
69. Chneiweiss, H., Glowinski, J. & Premont, J. Vasoactive intestinal polypeptide receptors linked to an adenylate cyclase, and their relationship with biogenic amine- and somatostatin-sensitive adenylate cyclases on central neuronal and glial cells in primary cultures. *J. Neurochem.* **44**, 779–786 (1985).
70. Hosli, E. & Hosli, L. Autoradiographic localization of binding sites for vasoactive intestinal peptide and angiotensin II on neurons and astrocytes of cultured rat central nervous system. *Neuroscience* **31**, 463–470 (1989).
71. Delgado, M. & Ganea, D. Vasoactive intestinal peptide: a neuropeptide with pleiotropic immune functions. *Amino Acids* **45**, 25–39 (2013).
72. Baer, G. M. et al. Sporadic FTLDP type C is a distinct clinicopathological entity from FTLDP types A/B (S7.007). *Neurology* **88**, S7.007 (2017).
73. Rohrer, J. D. et al. The heritability and genetics of frontotemporal lobar degeneration. *Neurology* **73**, 1451–1456 (2009).
74. Snowden, J., Neary, D. & Mann, D. Frontotemporal lobar degeneration: clinical and pathological relationships. *Acta Neuropathol.* **114**, 31–38 (2007).
75. Neary, D. et al. Frontotemporal lobar degeneration: a consensus on clinical diagnostic criteria. *Neurology* **51**, 1546–1554 (1998).
76. Younes, K. et al. Right temporal degeneration and socioemotional semantics: semantic behavioural variant frontotemporal dementia. *Brain* **145**, 4080–4096 (2022).
77. Acocella, G. & Billing, B. H. The effect of rifamycin SV on pigment excretion in rats. *Gastroenterology* **49**, 526–530 (1965).
78. Snowden, J. S. et al. Semantic dementia and the left and right temporal lobes. *Cortex* **107**, 188–203 (2018).
79. Josephs, K. A. et al. Two distinct subtypes of right temporal variant frontotemporal dementia. *Neurology* **73**, 1443–1450 (2009).
80. Kumfor, F. et al. On the right side? A longitudinal study of left-versus right-lateralized semantic dementia. *Brain* **139**, 986–998 (2016).
81. Chan, D. et al. The clinical profile of right temporal lobe atrophy. *Brain* **132**, 1287–1298 (2009).
82. Borghesani, V. et al. Regional and hemispheric susceptibility of the temporal lobe to FTLDP type C pathology. *Neuroimage Clin.* **28**, 102369 (2020).
83. Ulugut, H. et al. Clinical recognition of frontotemporal dementia with right anterior temporal predominance: a multi-center retrospective cohort study. *Alzheimers Dement.* **20**, 5647–5661 (2024).
84. Pan, L. et al. Transcription factor RBPJL is able to repress notch target gene expression but is non-responsive to notch activation. *Cancers* **13**, 5027 (2021).
85. Bonham, L. W. et al. Genetic variation across RNA metabolism and cell death gene networks is implicated in the semantic variant of primary progressive aphasia. *Sci. Rep.* **9**, 10854 (2019).
86. Lu, J. et al. L3MBTL1 regulates ALS/FTD-associated proteotoxicity and quality control. *Nat. Neurosci.* **22**, 875–886 (2019).
87. Guissart, C. et al. Premature termination codons in SOD1, causing amyotrophic lateral sclerosis, are predicted to escape the nonsense-mediated mRNA decay. *Sci. Rep.* **10**, 20738 (2020).
88. Murley, A. G. & Rowe, J. B. Neurotransmitter deficits from frontotemporal lobar degeneration. *Brain* **141**, 1263–1285 (2018).
89. Ferrer, I. Neurons and their dendrites in frontotemporal dementia. *Dement. Geriatr. Cogn. Disord.* **10**, 55–60 (1999).
90. Premi, E. et al. Unravelling neurotransmitters impairment in primary progressive aphasia. *Hum. Brain Mapp.* **44**, 2245–2253 (2023).
91. Bowen, D. M. et al. Imbalance of a serotonergic system in frontotemporal dementia: implication for pharmacotherapy. *Psychopharmacology* **196**, 603–610 (2008).
92. Procter, A. W., Qurne, M. & Francis, P. T. Neurochemical features of frontotemporal dementia. *Dement. Geriatr. Cogn. Disord.* **10**, 80–84 (1999).
93. Premi, E. et al. Early neurotransmitters changes in prodromal frontotemporal dementia: a GENFI study. *Neurobiol. Dis.* **179**, 106068 (2023).
94. Ghezzi, L., Cantoni, C., Rotondo, E. & Galimberti, D. The gut microbiome-brain crosstalk in neurodegenerative diseases. *Biomed.* **10**, 1486 (2022).
95. Khawar, M. M. Sr. et al. The gut-brain axis in autoimmune diseases: emerging insights and therapeutic implications. *Cureus* **15**, e48655 (2023).
96. Miller, Z. A. et al. TDP-43 frontotemporal lobar degeneration and autoimmune disease. *J. Neurol. Neurosurg. Psychiatry* **84**, 956–962 (2013).
97. Arseni, D. et al. Heteromeric amyloid filaments of ANXA11 and TDP-43 in FTLDP type C. *Nature* **634**, 662–668 (2024).
98. Arseni, D. et al. Structure of pathological TDP-43 filaments from ALS with FTLDP. *Nature* **601**, 139–143 (2022).
99. Arseni, D. et al. TDP-43 forms amyloid filaments with a distinct fold in type A FTLDP. *Nature* **620**, 898–903 (2023).
100. Brooks, B. R. El Escorial World Federation of Neurology criteria for the diagnosis of amyotrophic lateral sclerosis. Subcommittee on motor neuron diseases/amyotrophic lateral sclerosis of the World Federation of Neurology research group on neuromuscular diseases and the El Escorial “Clinical limits of amyotrophic lateral sclerosis” workshop contributors. *J. Neurol. Sci.* **124**, 96–107 (1994).
101. Olson, J. E. et al. The Mayo Clinic Biobank: a building block for individualized medicine. *Mayo Clin. Proc.* **88**, 952–962 (2013).
102. McPeck, M. S. & Sun, L. Statistical tests for detection of misspecified relationships by use of genome-screen data. *Am. J. Hum. Genet.* **66**, 1076–1094 (2000).
103. Willer, C. J., Li, Y. & Abecasis, G. R. METAL: fast and efficient meta-analysis of genomewide association scans. *Bioinformatics* **26**, 2190–2191 (2010).
104. Watanabe, K., Taskesen, E., van Bochoven, A. & Posthuma, D. Functional mapping and annotation of genetic associations with FUMA. *Nat. Commun.* **8**, 1826 (2017).
105. Lake, B. B. et al. Integrative single-cell analysis of transcriptional and epigenetic states in the human adult brain. *Nat. Biotechnol.* **36**, 70–80 (2018).
106. Allen, M. et al. Human whole genome genotype and transcriptome data for Alzheimer’s and other neurodegenerative diseases. *Sci. Data* **3**, 160089 (2016).
107. Mostafavi, S. et al. A molecular network of the aging human brain provides insights into the pathology and cognitive decline of Alzheimer’s disease. *Nat. Neurosci.* **21**, 811–819 (2018).
108. Bennett, D. A. et al. Religious orders study and rush memory and aging project. *J. Alzheimers Dis.* **64**, S161–S189 (2018).
109. Wang, M. et al. The Mount Sinai cohort of large-scale genomic, transcriptomic and proteomic data in Alzheimer’s disease. *Sci. Data* **5**, 180185 (2018).

110. Consortium, G. T. The GTEx consortium atlas of genetic regulatory effects across human tissues. *Science* **369**, 1318–1330 (2020).
111. Bryois, J. et al. Cell-type-specific cis-eQTLs in eight human brain cell types identify novel risk genes for psychiatric and neurological disorders. *Nat. Neurosci.* **25**, 1104–1112 (2022).
112. Young, A. M. H. et al. A map of transcriptional heterogeneity and regulatory variation in human microglia. *Nat. Genet.* **53**, 861–868 (2021).
113. Lopes, K. P. et al. Genetic analysis of the human microglial transcriptome across brain regions, aging and disease pathologies. *Nat. Genet.* **54**, 4–17 (2022).
114. Wingo, A. P. et al. Integrating human brain proteomes with genome-wide association data implicates new proteins in Alzheimer's disease pathogenesis. *Nat. Genet.* **53**, 143–146 (2021).
115. Ng, B. et al. An xQTL map integrates the genetic architecture of the human brain's transcriptome and epigenome. *Nat. Neurosci.* **20**, 1418–1426 (2017).
116. Alasoo, K. et al. Shared genetic effects on chromatin and gene expression indicate a role for enhancer priming in immune response. *Nat. Genet.* **50**, 424–431 (2018).
117. Nedelec, Y. et al. Genetic ancestry and natural selection drive population differences in immune responses to pathogens. *Cell* **167**, 657–669 e21 (2016).
118. Chen, L. et al. Genetic drivers of epigenetic and transcriptional variation in human immune cells. *Cell* **167**, 1398–1414 e24 (2016).
119. Momozawa, Y. et al. IBD risk loci are enriched in multigenic regulatory modules encompassing putative causative genes. *Nat. Commun.* **9**, 2427 (2018).
120. Quach, H. et al. Genetic adaptation and Neandertal admixture shaped the immune system of human populations. *Cell* **167**, 643–656 e17 (2016).
121. Fairfax, B. P. et al. Innate immune activity conditions the effect of regulatory variants upon monocyte gene expression. *Science* **343**, 1246949 (2014).
122. Kerimov, N. et al. A compendium of uniformly processed human gene expression and splicing quantitative trait loci. *Nat. Genet.* **53**, 1290–1299 (2021).
123. Edgar, R. D., Jones, M. J., Meaney, M. J., Turecki, G. & Kobor, M. S. BECon: a tool for interpreting DNA methylation findings from blood in the context of brain. *Transl. Psychiatry* **7**, e1187 (2017).
124. Mancuso, N. et al. Probabilistic fine-mapping of transcriptome-wide association studies. *Nat. Genet.* **51**, 675–682 (2019).

Acknowledgements

We thank the Mayo Clinic Center of Individualized Medicine for collection and sequencing of the Mayo Clinic Biobank samples. CG would also like to acknowledge Dr Inger Nennesmo for the neuropathological characterization. Acknowledgment for the ADSP dataset can be found in Supplementary Notes. This work was made possible by the support of funding from the UG3/UH3 NS103870 (RR), P30 AG062677 (BFB), P01 AG003949 (DWD), P01 NS084974 (DWD), R01 AG037491 (KAJ), R01 DC012519 (JLW), R21 NS94684 (KAJ), R01 DC010367 (KAJ), P30 AG062422 (JSY, WWS, BLM, HJR), P01 AG019724 (DHG, BLM, ALB, WWS), U01 AG057195 (BCD), P30 AG077444 (MMM), P30 AG013854 (MMM, SW), P30 AG07297, P30 AG066468 (OLL, JK), P30 AG012300 (CLW), P30 AG072972 (JL-W), P30 AG010129 (JL-W), P50 AG005136 (DCK), P30 AG066509 (DCK), P30 AG066511 (JG), P01 AG066597 (MG), P30 AG072979 (EBL, VVD), R01 NS085770 (CG), R01 AG091388 (TG, CG, MMM), and R01 DC008552 (MMM). It was further supported by the ALLFTD Consortium (U19: AG063911, funded by the NIA and NINDS, to BFB, DWD, ALB) and the former ARTFL & LEFFTDS Consortia (ARTFL: U54 NS092089, to ALB, funded by the NINDS and NCATS; LEFFTDS: U01 AG045390, funded by the NIA and NINDS, to BFB). It was also supported by the Mayo ADRC (P30 AG62677, funded by the NIA, to RCP). A subset of samples was obtained through the National Centralized Repository for

Alzheimer Disease and Related Dementias (NCRAD), which receives government support under a cooperative agreement grant (U24 AG021886) awarded by the National Institute on Aging (NIA), and was used in this study. ZKW was supported by Mayo Clinic Center for Regenerative Medicine, the gifts from the Donald G. and Jodi P. Heeringa Family, the Haworth Family Professorship in Neurodegenerative Diseases fund, the Albertson Parkinson's Research Foundation, and PPND Family Foundation. This work was further supported by the Rainwater Charitable Foundation (DWD, BFB, WWS, DHG, JSY) and the Bluefield Project to Cure FTD (RR and JDR), the DEC Brain and BioBank (ECF), CIHR grant 74580 (IRM), the Canadian Consortium on Neurodegeneration in Aging, of the Canadian Institutes of Health Research (IRM), the University of Pittsburgh Brain Institute (JK). JDR was further supported by the NIHR UCL/H Biomedical Research Centre, the UK MRC (MR/M008525/1; MR/M023664/1), and the JPND (2019-02248). CLW was supported, in part, by the Winspear Family Center for Research on the Neuropathology of Alzheimer disease, the McCune Foundation, and the Nancy and Buster Alvord endowment. CG was supported by Grants provided by Swedish FTD Initiative- Schörling foundation, the Swedish Research Council (Dnr 521-2010-3134, 529-2014-7504, 2015-02926), Alzheimer Foundation Sweden, Brain Foundation Sweden, Swedish Brain Power, Gamla Tjänarinnor, Stohnes Foundation, Dementia Foundation Sweden, and the Stockholm County Council (ALF-project). The brain pathology was provided through in part by the Brain Bank at Karolinska Institutet, which was financially supported by Karolinska Institutet StratNeuro, Swedish Brain Power, Stockholm County Council core facility funding (CG), and Schörling Foundation. KS was supported in part by SAO-FRA 2021/0032. FK is supported by a postdoctoral fellowship (BOF 49758) from the University of Antwerp Research Fund and a postdoctoral fellowship from Brein Instituut. RR was supported by a grant from the Fund for Scientific Research, Flanders (G064223N).

Author contributions

C.P., and R.R.: Study concept or design, acquisition of data, analysis or interpretation of data, statistical analysis or interpretation of data, drafting the manuscript for content, revising the manuscript for content, study supervision or coordination. M.B., F.K., A.B., G.D.J., J.M.B., C.L.D.: Sequencing, data analysis or interpretation of data, and drafting the manuscript for content, including writing of content. M.V.B., C.T.V., W.D.C., S.W., P.V.W., O.A.R., M.E.M., J.F., S.J.H., J.V.R., M.O.M., G.Y.R.H., C.G., L.Ö., M.N., Y.A., S.K.M., S.B., K.A.J., J.L.W.W., K.F.B., L.F., H.H., A.L.L., E.G.G., J.S.Y., A.P.O., M.F., Q.M., J.R.H., J.B.K., K.D.R., M.S., C.W., C.O., B.C.D., B.M.E., B.N.D., D.G.M., J.K., L.Z., E.R., E.S., T.G., C.G., S.W., J.D.S., M.R.F., D.E., B.K.W., R.J.C., L.L.K., E.D.H., E.M.R., S.M., A.K., S.R., A.L.N., N.E.T., D.S.K., R.C.P., L.P., R.J.U., Z.K.W., E.M.R., L.T.G., M.G.T., H.J.R., S.S., O.P., M.G., J.Q.T., D.C.K., J.L., J.P., D.H.G., R.A.R., C.C., B.G., G.M.H., T.G.B., G.E.S., T.A., J.H., A.L.B., L.S.H., J.P.V., O.L.L., J.K., C.L.W., M.G., J.G.L., J.D.R., D.J.I., E.B.L., V.V.D., R.C., M.M., M.C.T., E.C.F., C.T., S.A.F.S., B.L.M., H.S., N.G.R., B.F.B., I.R.A.M.K., J.C.V., W.W.S., K.S., and D.W.D.: Revised the manuscript for content, provided intellectual input and most shared samples. All authors: Read and approved the final manuscript.

Competing interests

S.J.H. serves on the scientific advisory board (SAB) of Proximity Therapeutics, Psy Therapeutics, Frequency Therapeutics, Souvien Therapeutics, Sensorium Therapeutics, 4 M Therapeutics, Ilios Therapeutics, Entheos Labs, Alzheimer's Drug Discovery Foundation, and the Kissick Family Foundation FTD Grant Program, none of whom were involved in the present study. S.J.H. has also received speaking or consulting fees from Amgen, AstraZeneca, Biogen, Merck, Regency Pharmaceuticals, Syros Pharmaceuticals, Juvenescence Life, as well as sponsored research or gift funding from AstraZeneca, JW Pharmaceuticals, Lexicon Pharmaceuticals, Vesigen Therapeutics, Compass Pathways, Atai Life Sciences, and Stealth Biotherapeutics. The funders had no role in the

design or content of this article. ZKW serves as PI or Co-PI on Biohaven Pharmaceuticals, Inc. (BHV4157-206), Vigil Neuroscience, Inc. (VGL101-01.002, VGL101-01.201, PET tracer development protocol, Csf1r biomarker and repository project, and ultra-high field MRI in the diagnosis and management of CSF1R-related adult-onset leukoencephalopathy with axonal spheroids and pigmented glia), and ONO-2808-03 projects/grants. He serves as Co-PI of the Mayo Clinic APDA Center for Advanced Research and as an external advisory board member for the Vigil Neuroscience, Inc., and as a consultant for Eli Lilly & Company and for NovoGlia, Inc. R.R. and I.R.M. receive royalties from progranulin-related patent. The remaining authors declare no competing interests.

Additional information

Supplementary information The online version contains supplementary material available at <https://doi.org/10.1038/s41467-025-59216-0>.

Correspondence and requests for materials should be addressed to Cyril Pottier or Rosa Rademakers.

Peer review information *Nature Communications* thanks Oriol Dols-Icardo, Celeste Sassi, Emilia Vitale, and the other, anonymous, reviewer(s) for their contribution to the peer review of this work. A peer review file is available.

Reprints and permissions information is available at <http://www.nature.com/reprints>

Publisher's note Springer Nature remains neutral with regard to jurisdictional claims in published maps and institutional affiliations.

Open Access This article is licensed under a Creative Commons Attribution-NonCommercial-NoDerivatives 4.0 International License, which permits any non-commercial use, sharing, distribution and reproduction in any medium or format, as long as you give appropriate credit to the original author(s) and the source, provide a link to the Creative Commons licence, and indicate if you modified the licensed material. You do not have permission under this licence to share adapted material derived from this article or parts of it. The images or other third party material in this article are included in the article's Creative Commons licence, unless indicated otherwise in a credit line to the material. If material is not included in the article's Creative Commons licence and your intended use is not permitted by statutory regulation or exceeds the permitted use, you will need to obtain permission directly from the copyright holder. To view a copy of this licence, visit <http://creativecommons.org/licenses/by-nc-nd/4.0/>.

© The Author(s) 2025

Cyril Pottier^{1,2,3,4,5}✉, Fahri Küçükali^{2,3}, Matt Baker¹, Anthony Batzler⁶, Gregory D. Jenkins⁶, Marka van Blitterswijk¹, Cristina T. Vicente^{2,3}, Wouter De Coster^{2,3}, Sarah Wynants^{2,3}, Pieter Van de Walle^{2,3}, Owen A. Ross¹, Melissa E. Murray¹, Júlia Faura^{2,3}, Stephen J. Haggarty⁷, Jeroen G.J. van Rooij⁸, Merel O. Mol⁸, Ging-Yuek R. Hsiung⁹, Caroline Graff^{10,11}, Linn Öjjerstedt^{10,11}, Manuela Neumann^{12,13}, Yan Asmann¹⁴, Shannon K. McDonnell⁶, Saurabh Baheti⁶, Keith A. Josephs¹⁵, Jennifer L. Whitwell¹⁶, Kevin F. Bieniek^{1,17}, Leah Forsberg¹⁵, Hilary Heuer¹⁸, Argentina Lario Lago¹⁸, Ethan G. Geier¹⁸, Jennifer S. Yokoyama¹⁸, Alexis P. Oddi¹⁸, Margaret Flanagan¹⁷, Qinwen Mao¹⁹, John R. Hodges²⁰, John B. Kwok^{21,22}, Kimiko Domoto-Reilly²³, Matthis Synofzik^{12,24}, Carlo Wilke^{12,24}, Chiadi Onyike²⁵, Bradford C. Dickerson²⁶, Bret M. Evers²⁷, Brittany N. Dugger²⁸, David G. Munoz^{29,30}, Julia Keith^{30,31}, Lorne Zinman³¹, Ekaterina Rogaeva³², EunRan Suh³³, Tamar Gefen³⁴, Changiz Geula³⁴, Sandra Weintraub³⁴, Janine Diehl-Schmid^{35,36}, Martin R. Farlow³⁷, Dieter Edbauer³⁸, Bryan K. Woodruff³⁹, Richard J. Caselli³⁹, Laura L. Donker Kaat⁴⁰, Edward D. Huey⁴¹, Eric M. Reiman⁴², Simon Mead⁴³, Andrew King^{44,45}, Sigrun Roeber⁴⁶, Alissa L. Nana¹⁸, Nilufer Ertekin-Taner^{1,47}, David S. Knopman¹⁵, Ronald C. Petersen¹⁵, Leonard Petrucelli¹, Ryan J. Uitti⁴⁷, Zbigniew K. Wszolek⁴⁷, Eliana Marisa Ramos⁴⁸, Lea T. Grinberg¹⁸, Maria Luisa Gorno Tempini¹⁸, Howard J. Rosen⁴⁹, Salvatore Spina¹⁸, Olivier Piguet⁵⁰, Murray Grossman^{51,73}, John Q. Trojanowski^{33,74}, C. Dirk Keene⁵², Lee-Way Jin⁵³, Johannes Prudlo^{54,55}, Daniel H. Geschwind⁴⁸, Robert A. Rissman⁵⁶, Carlos Cruchaga⁵⁷, Bernardino Ghetti⁵⁸, Glenda M. Halliday²¹, Thomas G. Beach⁵⁹, Geidy E. Serrano⁵⁹, Thomas Arzberger^{46,60}, Jochen Herms^{38,46}, Adam L. Boxer¹⁸, Lawrence S. Honig⁶¹, Jean P. Vonsattel⁶², Oscar L. Lopez⁶³, Julia Kofler⁶⁴, Charles L. White III²⁷, Marla Gearing⁶⁵, Jonathan Glass⁶⁵, Jonathan D. Rohrer⁶⁶, David J. Irwin⁵¹, Edward B. Lee³³, Vivianna Van Deerlin³³, Rudolph Castellani⁶⁷, Marsel M. Mesulam³⁴, Maria C. Tartaglia³², Elizabeth C. Finger⁶⁸, Claire Troakes⁴⁴, Safa Al-Sarraj^{44,69}, Clifton L. Dalgard⁷⁰, Bruce L. Miller¹⁸, Harro Seelaar⁸, Neill R. Graff-Radford⁴⁷, Bradley F. Boeve¹⁵, Ian R.A. Mackenzie⁷¹, John C. van Swieten⁸, William W. Seeley¹⁸, Kristel Slegers^{2,3}, Dennis W. Dickson¹, Joanna M. Biernacka^{6,72} & Rosa Rademakers^{1,2,3}✉

¹Department of Neuroscience, Mayo Clinic, Jacksonville, FL, USA. ²Department of Biomedical Sciences, University of Antwerp, Antwerp, Belgium. ³VIB Center for Molecular Neurology, VIB, Antwerp, Belgium. ⁴Department of Neurology, Washington University School of Medicine, St Louis, MO, USA. ⁵NeuroGenomics and Informatics Center, Washington University School of Medicine, St Louis, MO, USA. ⁶Department of Quantitative Health Sciences, Mayo Clinic, Rochester, MN, USA. ⁷Department of Neurology, Massachusetts General Hospital and Harvard Medical School, Boston, MA, USA. ⁸Department of Neurology, Erasmus Medical Center, Rotterdam, The Netherlands. ⁹Department of Medicine, Division of Neurology, University of British Columbia, Vancouver, BC, Canada. ¹⁰Division of Neurogeriatrics, Karolinska Institutet, Solna, Sweden. ¹¹Unit for Hereditary Dementias, Karolinska University Hospital, Solna, Sweden. ¹²German Center for Neurodegenerative Diseases (DZNE), Tübingen, Germany. ¹³Department of Neuropathology, University of Tübingen, Tübingen, Germany. ¹⁴Department of Health Sciences Research, Mayo Clinic, Jacksonville, FL, USA. ¹⁵Department of Neurology, Mayo Clinic, Rochester, MN, USA. ¹⁶Department of

Radiology, Mayo Clinic, Rochester, MN, USA. ¹⁷University of Texas Health Science Center San Antonio, San Antonio, TX, USA. ¹⁸Department of Neurology, UCSF Weill Institute for Neurosciences, University of California, San Francisco, CA, USA. ¹⁹Department of Pathology, University of Utah, Salt Lake City, UT, USA. ²⁰Central Clinical School and Brain and Mind Centre, University of Sydney, Sydney, NSW, Australia. ²¹University of Sydney, Sydney, NSW, Australia. ²²NeuRA, University of New South Wales, Randwick, NSW, Australia. ²³Department of Neurology, University of Washington, Seattle, WA, USA. ²⁴Division Translational Genomics of Neurodegenerative Diseases, Center for Neurology and Hertie-Institute for Clinical Brain Research, University of Tübingen, Tübingen, Germany. ²⁵Department of Psychiatry and Behavioral Sciences, Johns Hopkins University, Baltimore, MD, USA. ²⁶Department of Neurology, Case Western Reserve University, Cleveland, OH, USA. ²⁷Division of Neuropathology, University of Texas Southwestern Medical Center, Dallas, TX, USA. ²⁸Department of Pathology and Laboratory Medicine, University of California, Davis Medical Center, Sacramento, CA, USA. ²⁹St. Michael's Hospital, Toronto, ON, Canada. ³⁰Department of Laboratory Medicine and Pathobiology, University of Toronto, Toronto, ON, Canada. ³¹Sunnybrook Health Sciences Centre, Toronto, ON, Canada. ³²Kremlin Discovery Tower, Tanz Centre for Research in Neurodegenerative Disease, University of Toronto, Toronto, ON, Canada. ³³Department of Pathology and Laboratory Medicine, Center for Neurodegenerative Disease Research, Perelman School of Medicine at the University of Pennsylvania, Philadelphia, PA, USA. ³⁴Mesulam Center for Cognitive Neurology and Alzheimer's Disease, Northwestern University, Chicago, IL, USA. ³⁵Department of Psychiatry and Psychotherapy, Technical University of Munich, Munich, Germany. ³⁶kbo-Inn-Salzach-Klinikum, Clinical Center for Psychiatry, Psychotherapy, Psychosomatic Medicine, Geriatrics and Neurology, Wasserburg/Inn, Germany. ³⁷Department of Neurology, Indiana University School of Medicine, Indianapolis, IN, USA. ³⁸German Center for Neurodegenerative Diseases (DZNE), Munich, Germany. ³⁹Department of Neurology, Mayo Clinic, Scottsdale, AZ, USA. ⁴⁰Department of Clinical Genetics, Erasmus Medical Center, Rotterdam, The Netherlands. ⁴¹Department of Psychiatry and Human Behavior, Brown Alpert Medical School, Brown University, Providence, RI, USA. ⁴²Banner Alzheimer's Institute, Phoenix, AZ, USA. ⁴³MRC Prion Unit at University College London, Institute of Prion Diseases, London, UK. ⁴⁴Department of Basic and Clinical Neuroscience, London Neurodegenerative Diseases Brain Bank, Institute of Psychiatry, Psychology and Neuroscience, King's College London, London, UK. ⁴⁵Department of Clinical Neuropathology, King's College Hospital NHS Foundation Trust, London, UK. ⁴⁶Centre for Neuropathology and Prion Research, Ludwig-Maximilians-University of Munich, Munich, Germany. ⁴⁷Department of Neurology, Mayo Clinic, Jacksonville, FL, USA. ⁴⁸Department of Neurology, David Geffen School of Medicine, University of California, Los Angeles, CA, USA. ⁴⁹Department of Pathology, UCSF Weill Institute for Neurosciences, University of California, San Francisco, CA, USA. ⁵⁰School of Psychology and Brain and Mind Centre, University of Sydney, Sydney, NSW, Australia. ⁵¹Department of Neurology, Penn Frontotemporal Degeneration Center, Perelman School of Medicine at the University of Pennsylvania, Philadelphia, PA, USA. ⁵²University of Washington BioRepository and Integrated Neuropathology (BRaIN) lab, Harborview Medical Center, Seattle, WA, USA. ⁵³M.I.N.D. Institute Laboratory, University of California, Davis Medical Center, Sacramento, CA, USA. ⁵⁴German Center for Neurodegenerative Diseases (DZNE), Rostock, Germany. ⁵⁵Department of Neurology, Rostock University Medical Center, Rostock, Germany. ⁵⁶Alzheimer's Therapeutic Research Institute, Keck School of Medicine of the University of Southern California, San Diego, CA, USA. ⁵⁷Department of Psychiatry, Knight Alzheimer Disease Research Center, Washington University School of Medicine, Saint Louis, MO, USA. ⁵⁸Department of Pathology and Laboratory Medicine, Indiana University School of Medicine, Indianapolis, IN, USA. ⁵⁹Civin Laboratory for Neuropathology, Banner Sun Health Research Institute, Sun City, AZ, USA. ⁶⁰Department of Psychiatry and Psychotherapy, University Hospital, Ludwig-Maximilians-University of Munich, Munich, Germany. ⁶¹Department of Neurology, Taub Institute for Research on Alzheimer's Disease and the Aging Brain, Columbia University Irving Medical Center, New York, NY, USA. ⁶²Department of Pathology, Taub Institute for Research on Alzheimer's Disease and the Aging Brain, Columbia University Irving Medical Center, New York, NY, USA. ⁶³Department of Neurology, University of Pittsburgh, Pittsburgh, PA, USA. ⁶⁴Department of Pathology, University of Pittsburgh, Pittsburgh, PA, USA. ⁶⁵Department of Pathology and Laboratory Medicine and Department of Neurology, Emory University, Atlanta, GA, USA. ⁶⁶Department of Neurodegenerative Disease, Dementia Research Centre, University College London, Queen Square Institute of Neurology, London, UK. ⁶⁷Department of Pathology, Feinberg School of Medicine, Northwestern University, Chicago, IL, USA. ⁶⁸Department of Clinical Neurological Sciences, Schulich School of Medicine and Dentistry, University of Western Ontario, London, ON, Canada. ⁶⁹King's College Hospital NHS Foundation Trust, London, UK. ⁷⁰Department of Anatomy, Physiology and Genetics, Uniformed Services University of the Health Sciences, Bethesda, MD, USA. ⁷¹Department of Pathology and Laboratory Medicine, University of British Columbia, Vancouver, BC, Canada. ⁷²Department of Psychiatry & Psychology, Mayo Clinic, Rochester, MN, USA. ⁷³Deceased: Murray Grossman. ⁷⁴Deceased: John Q. Trojanowski. ✉ e-mail: cpottier@wustl.edu; rosa.rademakers@uantwerpen.vib.be